Fluctuation dynamics of bilayer vesicles with intermonolayer sliding: Experiment and Theory

Michael Mell,[1,§] Lara H. Moleiro,[1,2,§] Yvonne Hertle,[3]
Iván López-Montero,[1] Francisco J. Cao,[4] Peter Fouquet,[5]
Thomas Hellweg[3] and Francisco Monroy.[1,*]

[1] *Departamento de Química Física I, Universidad Complutense de Madrid, E-28040 Madrid, Spain, EU*

[2] *Physikalische Chemie I, Univeristät Bayreuth, Universitätsstraße 30, D-95447 Bayreuth, Germany, EU*

[3] *Physikalische und Biophysikalische Chemie I, Universität Bielefeld, Universitätsstraße 25, D-33615 Bielefeld, Germany, EU*

[4]*Departamento de Física Atómica, Molecular y Nuclear, Universidad Complutense de Madrid, E-28040 Madrid, Spain, EU*

[5]*TOF/HR Group, Institut Laue Langevin, 6 rue Jules Horowitz, BP156, F-38042 Grenoble Cedex 9, France, EU*

Submitted to Chem Phys Lipids (Special Issue on Membrane Mechanics), on September 3rd, 2014

Revised on:

* Corresponding addresses: monroy@quim.ucm.es

§ These two authors contributed equally to this work and should be considered co-first authors

Abstract

The presence of coupled modes of membrane motion in closed shells is extensively predicted by theory. The bilayer structure inherent to lipid vesicles is suitable to support hybrid modes of curvature motion coupling membrane bending with the local reorganization of the bilayer material through relaxation of the dilatational stresses. Previous experiments evidenced the existence of such hybrid modes facilitating membrane bending at high curvatures in lipid vesicles [Rodríguez-García et al. Phys. Rev. Lett. 102, 128201 (2009)]. For lipid bilayers that are able to undergo intermonolayer sliding, the experimental fluctuation spectra are found compatible with a bimodal schema. The usual tension/bending fluctuations couple with the hybrid modes in a mechanical interplay, which becomes progressively efficient with increasing vesicle radius, to saturate at infinity radius into the behavior expected for a flat membrane. Grounded on the theory of closed shells, we propose an approximated expression of the bimodal spectrum, which predicts the observed dependencies on the vesicle radius. The dynamical features obtained from the autocorrelation functions of the vesicle fluctuations are found in quantitative agreement with the proposed theory.

Keywords: lipid, membrane, bending, friction

I. INTRODUCTION

Biological membranes are dynamic closed shell assemblies structurally based on the lyotropic self-organization as fluid lipid bilayers [1,2]. The fluid lipid bilayer is composed of two monomolecular sheets, which are intrinsically characterized by a strong lateral cohesion and held together by weak van der Waals forces. Transverse and lateral forces in the bilayer are significant, since they not only determine cell shapes [3,4,5] but also membrane dynamics [6,7,8]. Deformation modes in lipid membranes are governed by the mechanical properties of the bilayer, their dynamics being relevant at the time scale determined by the different dissipation mechanisms present in the system [9,10,11,12]. In general, the mechanical response of a fluid lipid bilayer should occur through curvature deflections and stretching deformations. Curvature deflections are transverse motions, which define shape changes through two relevant rigidities: the surface tension (σ) and the bending modulus (κ) [13]. The surface tension dominates the energy of the flexural deformations put into play through the excess area of the membrane, whereas the bending rigidity determines the strength of the net change in curvature with respect to the equilibrium conformation. Pure longitudinal motions are governed by the compression modulus of the constituting monolayers (K) [14]. Exposed to lateral strain, lipid membranes are quite rigid as compared to flexural deformations, which is an inherent characteristic of the bilayer packing leading to its high mechanical stability. Consequently, net area changes are considered to be suppressed in lipid membranes, due to the large energy penalty associated to. Hence, the membrane area is usually assumed a system invariant in lipid bilayers. Ideally, lipid bilayers are considered as 2D-sheets characterized by a low tension, small bending resistance and global lateral incompressibility, a set of mechanical characteristics making them to behave as floppy membranes susceptible to undergo shape changes with very limited

longitudinal deformation. The standard Helfrich's treatment of the fluctuating single-sheet membrane leads to a monomodal spectrum of the thermal curvature fluctuations exclusively governed by surface tension and bending forces [13]. In the real thing, which is actually a bilayer with a finite thickness, however, a local deflection might cause a longitudinal reorganization of the lipid material in each monolayer. Particularly, one expects a dilation in the outer monolayer followed by an equivalent compression in the inner one as consequence of any change of curvature of the membrane. The extended theory of the composite bilayer membrane was seminally formulated by Helfrich [15], and later put forward by Evans end Yeung [16,17]. This theory predicts the existence of coupled dilational-curvature modes supported by the bilayer structure, in addition to the pure flexural modes, a fact that has been recognised as crucial to understand membrane energetics [18]. Those coupled dilational-curvature stresses could become eventually relaxed by possible interbilayer transport and the energy dissipated by intra-/inter-monolayer friction, thus appearing a degree of freedom additional to the pure flexural mode, which is usually referred to as hybrid mode. In the limit of free slippage, except for the intrinsic viscous resistance of the lipid monolayers, they are free to slide relative to one another giving rise to a fast hybrid mode dynamically coupled within the density modes of the bilayer structure. The Helfrich's description formally corresponds to a planar sheet with free edges, thus no lateral compression deformations are drawn upon small bending. However, flexible membranes in a closed shell topology, e.g. bilayer lipid vesicles, represent a different elastic problem where curvature deformations necessarily imply a dilation of the membrane.

Here, we address the question of how curvature deformations in a lipid bilayer vesicle could efficiently couple with longitudinal dilations occurring in the constituting monolayers. Such a coupling should provide an enhanced local deformability [15],

mainly at highly curved regions where bending deformations could somewhat become governed by lateral intrabilayer stresses. On the one hand, an enhanced coupling is expected in closed membranes of curved vesicles, resulting in a certain influence of the hybrid dilatation-curvature modes on the global shape fluctuations [19]. The effect is so important that even for slightly curved vesicles ($R/h >> 1$), thermal fluctuations are expected with an increased amplitude at low wavevectors ($qR \approx 1$) [19]. On the other hand, no strong influence of the hybrid modes should occur in large vesicles ($R \rightarrow \infty$), where large-scale lateral motions are expected to release longitudinal stresses in a very efficient way, similarly to flat-bilayers with free edges.

Intermonolayer friction affects dilation-curvature coupling in bilayer systems. Previous experiments with bilayer vesicles have demonstrated the effect of interlayer coupling in membrane mechanics through the influence of intermonolayer friction on their relaxation dynamics [20,21,22,23]. Additional evidence of intermonolayer coupling was demonstrated in tether pulling experiments [24] and from its retarding effect on the lateral diffusion of fluorescent probes [25]. With regard to dissipation dynamics, theoretical analyses by Seifert and cols. [26,27] have shown that the two dissipative mechanisms, namely conventional bulk friction and intermonolayer drag, are important on different length scales. Whereas the single-sheet Helfrich's theory of membrane fluctuations is monomodal (flexural mode only), the extended theory demonstrates the existence of different fluctuation modes undergoing different dissipative pathways [10,26,27]: 1) Pure flexural mode, which is restored by membrane tension (σ) and bending curvature (κ) and dissipates through bulk friction. 2) Pure dilational mode, governed by lateral compression elasticity (K) and monolayer viscosities. 3) Hybrid dilation-curvature, which couples flexural deformations with lateral dilations. For this hybrid mode, the restoring force is accounted for by the

compression modulus (K), and the viscous dissipation by the intermonolayer friction (b). Transverse motions are caused by both, the pure flexural mode (1) and the hybrid dilation-curvature mode (3), which appear merged as two normal modes in a bimodal distribution of flexural modes [27]. Separately, the pure dilational mode (2), which is the third normal mode of the composite membrane problem, appears completely decoupled from the others. In addition, this pure dilational mode is "hidden" to usual experimental methods based on the tracking of the shape fluctuations, which exclusively "see" membrane deflections. Because every fluctuation mode is dominated by different energetics and different dissipative hydrodynamics, they might appear dynamically separated with different relative amplitudes depending on the scale probed. For long wavelength fluctuations, for which membrane tension dominates, viscous relaxation is barely governed by bulk viscosity [22], as predicted by the conventional MS theory of the membrane fluctuations [8]. From the extended theory [26,27,28], it is concluded that viscous resistance to curvature changes should be dominated by interlayer dissipation in the mesoscopic regime. In this regime, coupling between the ordinary bending mode and the hybrid dilation-curvature mode stands, producing a dynamic exchange of energy between the modes that cause the enhancement of the flexural deformations of the membrane [26,27]. In the limit of total adhesion between the monolayers, the membrane behaves as a uniform plate with a bending rigidity that obeys the relationship $\kappa_{mon} = (h^2/12)\, K$ [30], which drops to the bilayer value $\kappa_{bil} = (h^2/48)\, K$ ($= \kappa_{mon}/4$) if the plate is sliced into two leaflets free to slide past each other [14]. Mutual monolayer interdigitation leading to intermediate intermonolayer friction is accounted for by the "polymer brush" model [29], which predicts the intermediate result $\kappa_{brush} = (h^2/24)\, K$. These models of intermonolayer coupling lead, depending on the degree of intermonolayer friction, to a generalized bending rigidity $\kappa = h^2 K/\alpha$,

where the numerical constant α spans from: $\alpha = 12$ for total monolayer sticking, up to $\alpha = 48$, for ideal sliding. From a structural standpoint, chain interdigitation at the bilayer midplane causes mechanical coupling between the two monolayers. Such a structural coupling might determine the compositional dependence of the coupling constant α. Therefore, the degree of intermonolayer coupling not only determines the velocity differences between the two monolayers, leading to subsequent viscous friction, but also modifies the actual value of the bending rigidity. In qualitative terms: the weaker the coupling between the monolayers, the softer the membrane when stressed upon bending and the lower the intermonolayer friction. Therefore, if the sliding between the monolayers increases, then, the lateral redistribution of the lipid material is favored and the coupling between curvature and dilation enhanced. Consequently, the pathway for optimal coupling is open in bilayers with a reduced lipid interdigitation or a limited material transport between the monolayers. In these cases, the hybrid mode is favored and intermonolayer friction becomes the dominant dissipative mechanism. Regarding thermal fluctuations in the bilayer membrane, both modes, pure flexural and hybrid dilation-curvature, cause larger curvature deflections on the membrane than expected, which contribute to the enhanced shape fluctuations of the vesicle. Specifically, for a vesicle shell of radius *R*, both modes of deformation are first-order coupled, *i.e.* $\rho \sim \zeta/R$ [30], thus dilational effects might become significant even at small amplitudes of the shape deformations.

Vesicle fluctuation dynamics. The fluctuation dynamics of lipid vesicles spans many different spatiotemporal domains, ranging from the macroscopic scale, where the shape fluctuations can be directly observed under the optical microscope, down to the molecular scale. In the microscopic scale, a combination of inelastic neutron scattering [31] and molecular dynamics (MD) simulation [32,33] offers a congruent description of

the molecular structure and the fundamental transport process involved in the mechanical response of the lipid bilayer. In the macroscopic regime, flickering spectroscopy (FS) provides an inestimable tool to probe membrane dynamics both in giant unilamellar vesicles (GUVs) and in real cells [34]. In the hydrodynamic domain, at high wavevectors below a molecular cut-off, a continuous elasticity approach is still possible. There, inelastic scattering data from the undulating bilayer can be modeled as a dynamic form factor engendered by the shape fluctuations. In a seminal paper, the case of floppy membranes governed by pure-bending was addressed by Zilman and Granek (ZG) [35]. They have provided an accurate theory for such a dynamic structure factor [36], namely an intermediate scattering function. ZG showed that, when governed by bending elasticity, the intermediate scattering function of the membrane fluctuations decays as a stretched exponential at short length and time scales. Such a decay has been observed in experiments on microemulsion systems [37,38,39], lamellar bilayer phases [40,41] and vesicles [22,23,31,42,43]. However, a similar theory for hybrid curvature-dilational modes is still lacking. In the case of lipid bilayers with sliding monolayers, at the high curvatures probed by neutron scattering, a dominant influence of the hybrid modes is expected [23,31], revealing the need for a detailed dynamic theory of scattering from such a special class of membrane fluctuations.

In this paper, we contribute to resolve this problem by addressing a heuristic approach to the minimal mechanical theory of the locally compressible vesicle membrane through the assumption of hybrid modes coexisting with pure-bending motion in the shell topology. Experimentally, we consider shell membranes with a variable curvature by preparing unilamellar vesicles with different radii in the nano-/micro-meter size range. Furthermore, an extension of the ZG theory of scattering by membrane fluctuations governed by hybrid modes is delivered by this work, being revealed as an analytic

formulation adequate to exploit NSE data obtained with bilayer vesicles. Taking advantage of combined measurements with flickering spectroscopy and neutron spin echo with vesicles of different sizes, we provide experimental evidence concerning the radius-dependent influence of longitudinal motions on the curvature fluctuations.

II. THEORY

II-1. Planar membranes

a) Bending modes in an incompressible sheet. If a 2D-membrane sheet is considered laterally incompressible, thus longitudinal motions can be neglected. Consequently, its mechanical state is finally defined by the transverse deformations with respect to an equilibrium configuration. In the usual description, the free energy of the deformed sheet is given by the Canham-Helfrich Hamiltonian [44]; referred to the Monge-gauge, where ζ represents the local membrane deflection with respect to the flat reference plane [14], the mechanical energy due to transversal deflections (per unit area, *A*) is:

$$\delta F_T(\zeta) = \frac{1}{2}\left[\sigma(\nabla\zeta)^2 + \kappa\left(\nabla^2\zeta\right)^2\right] dA \qquad (1)$$

which assumes harmonic deformations; so, for small displacements, the changes in area and in curvature are accounted for as $\delta A/A \approx \nabla\zeta$ and $\delta C \approx \nabla^2\zeta$, respectively.

For this Hamiltonian, the standard treatment of the thermal fluctuations gives rise to an amplitude spectrum exclusively governed by surface tension (σ) and bending elasticity (κ) [13,14]; in *k*-space, the root mean squared (rms) amplitudes of the membrane fluctuations are given as:

$$\left\langle \zeta_k^2 \right\rangle = A^{-1} \frac{k_B T}{\sigma k^2 + \kappa k^4} \qquad (2)$$

where k is the modulus of the planar wavevector of the membrane fluctuation mode, $\zeta_k(x) \sim e^{ikx}$.

Regarding the dynamics of the membrane modes, bulk friction is assumed to be the main friction mechanism [7,8,45]. Considering linear hydrodynamics [7], transverse correlations are expected to relax following a single exponential profile:

$$\left\langle \zeta_{\mathbf{k}}(t)\zeta_{-\mathbf{k}}(0)\right\rangle = \left\langle \zeta_k^2 \right\rangle \exp\left(-\gamma_T t\right) \tag{3}$$

with a decay rate:

$$\gamma_T = \frac{\sigma k + \kappa k^3}{4\eta} \tag{4}$$

where η is the bulk viscosity.

b) Longitudinal strain caused by normal deflections in thin plates. Now, we will focus on the case of bending deflections in a flat membrane with a finite thickness h, considered thin as compared with its lateral dimensions ($h << A^{1/2}$) [30]. In this case, when the plate is bent and one looks at the interior, it appears stretched at the convex side and compressed at the concave one. As we penetrate into the plate, the strain field becomes progressively small and it exists a neutral plane where it exactly equals zero [30]. This neutral plane defines a internal surface which determines, even for a homogeneous material, a virtual bilayer structure. If a Cartesian coordinate system is located with the origin on the neutral surface and the z-axis normal to the surface, one can define the normal deflection as the vertical displacement of a point on the neutral surface, *i.e.* the normal deflection $u_z = \zeta(x,y)$. Since the plate is thin, comparatively small forces that are caused as a consequence of dilation are necessary to bend it. Consequently, the normal components of the stress tensor are small compared with the remaining in-plane components ($\sigma_{iz} << \sigma_{ij}$) [30]. The smallness of the off-plane stresses defines a very important elastic property of thin plates usually referred to as the

"hypothesis of straight normals" [46], which imposes negligible shear strains with respect to the normal deflection, this is $u_{zz} >> u_{iz} \approx 0$ [30,46]. From this assumption, the changes on the longitudinal fields along the *z*-direction can be easily calculated in terms of the normal deflection as $\partial u_i/\partial z \approx -\partial u_z/\partial x_i = -\partial\zeta/\partial x_i$; after integration along the *z*-direction and applying the chain rule, the relevant longitudinal components of the strain field in the weakly-bent thin sheet can be expressed as [30]:

$$u_{ii}^{(pl)} = \frac{\partial u_i}{\partial x_i} = z\frac{\partial^2 \zeta}{\partial x_i^2} \tag{5}$$

which are intrinsically zero at the neutral surface ($u_{xx} = u_{yy} = 0$ at $z = 0$).

The weak dilation produced by a small bending deflection is a property typical of linear deformations in thin plates ($\zeta \approx h$); for a macroscopic membrane ($A >> h^2$), one has $u^{(1)} \approx h\zeta/A \rightarrow 0$ [30]. However, for larger deflections ($\zeta >> h$), bending implies second-order effects on the dilation, $u_{\pm} \approx \pm(1/2)(\partial\zeta/\partial x)^2$, which should turn in the relevant stretching contribution to the height deformations of thin plates [30]. Therefore, any anharmonic description of the planar membrane would account for such non-linear dilational coupling, which intrinsically dominates the large deflections. In this regime ($\zeta >> h$), the second order dilation associated to the bending deflection varies as $u^{(2)} \approx \zeta^2/A$, a value much higher indeed than the linear deformation, *i.e.* $u^{(2)}/u^{(1)} \approx \zeta/h >> 1$ [30]. Such a nonlinear extension of the dynamics of the planar membrane is still awaiting theoretical development and experimental verification.

c) Hybrid curvature-dilation modes in bilayer membranes. Similarly to deformable plates with a finite thickness, in bilayer membranes, transverse bending deformations are necessarily accompanied by lateral displacements of the two monolayers [15,16,17]. In this case, local curvature should cause one leaflet to dilate while compressing the other, a structural change that could impart relevant functional consequences. In this

mechanism, the relevant time scale is determined essentially by intermonolayer friction, and by subsidiary interbilayer transport processes, namely, flip-flop motions. The notion of coupled curvature-dilation motion was exploited by Seifert et al. [16,17] to postulate a hybrid class of curvature motion allowing a softer pathway (energetically favored) than the pure bending motions. Intrinsically, such a hybrid curvature-dilation motion engenders a difference between the lipid density of each monolayer $\delta\rho$, which is defined with respect to the average value as $\delta\rho = (\rho_+ - \rho_-)/\rho_0$. When the membrane is curved, the densities $\rho_\pm$ differ from the equilibrium value ρ_0 in a way such that each monolayer dilates by the amount u ($=\delta A/A$) = $\delta\rho$. Such an effect was early recognized by Helfrich as a constitutive relation of spontaneous curvature in lipid bilayers [15]. In a linear approach, a given curvature is assumed to cause a proportional imbalance in the lipid densities between the two monolayers. On the idea that thicker membranes give rise to higher density differences, Helfrich assumed a linear relationship between the change in curvature and the density difference, $\delta\rho = (h/2)\delta C$ [15], h being the thickness of the bilayer. Because a curvature change in the planar membrane is described as $\delta C = \nabla^2\zeta$, the strain field defined in Eq. 5 is compatible with Helfrich's rule for a bilayer membrane with monolayer thickness $h/2$ [15], this is $u_\pm \approx \pm(h/2)\,\delta C$. Because they are restored by the compression elasticity of the constituting monolayers (K), hybrid motions contribute to the elastic Hamiltonian of the planar membrane, $\delta F = \delta F_T + \delta F_{hyb}$, as [16,17]:

$$\delta F_{hyb}(\zeta,\rho) = \frac{1}{2}K\left[\left(\rho_+ + \frac{h}{2}\nabla^2\zeta\right)^2 + \left(\rho_- - \frac{h}{2}\nabla^2\zeta\right)^2\right]dA \qquad (6)$$

Actually, the hybrid curvature-dilatational motions constitute a different type of membrane mode other than pure bending motions. Indeed, in a fluid membrane with free edges, longitudinal stresses produced by local curvatures could eventually relax by

lateral lipid flow. Thus, in the flat geometry considered by Seifert, hybrid modes appeared effectively uncoupled from the pure bending modes [16,17]. Consequently, no net contribution from hybrid modes is expected to the averaged transversal deflections in the flat membrane with free edges. In *k*-space, for a flat membrane patch of area *A*, the rms amplitude of the hybrid modes is [16,17]:

$$\left\langle \zeta_{\mathbf{k}} \rho_{-\mathbf{k}} \right\rangle = A^{-1} \frac{6}{h} \frac{k_B T}{K k^2} \tag{7}$$

which decreases with membrane thickness as h^{-1}.

From a dynamical standpoint, because each lipid monolayer differs in density from the other ($\rho_+ > \rho_-$), they thus flow at different velocities. Consequently, the resultant velocity gradient enforces a new dissipation mechanism dominated by intermonolayer friction. If hybrid modes are considered to mainly dissipate through frictional sliding between the monolayers, the corresponding relaxation rate is found to be [16,17]:

$$\gamma_{hyb} = \frac{K}{2b} k^2 \tag{8}$$

where *b* is the intermonolayer friction coefficient.

II-2. Curved bilayers: pure and hybrid modes in unilamellar vesicles.

The spherical problem was seminally addressed by Yeung and Evans [16], who early recognized the dynamic coupling intrinsic to the bilayer to impose new physics absent from the simpler description as a unit membrane. Such an intrinsic elasticity, namely a curvature-dilation coupling, should emerge as a relevant mechanism for the relaxation of the longitudinal stresses appearing upon local deflections. If the stress profile inside the bilayer is modeled by two thin, extensible monolayer shells at a distance *d* (= *h*/4) from the neutral plane, the intrinsic value of the curvature modulus is given by [15,47]:

$$\kappa_{int} = \frac{h^2}{24} K \tag{9}$$

where *K* is the compression modulus for one of the monolayers.

On the base that sliding between monolayers produces viscous drag at the bilayer midplane, the frictional coupling between the monolayers is identified as an effective mechanism to create additional dynamic impedance superposed to the usual hydrodynamic resistance of the bulk medium [10,17]. Differently to flat membranes, there are no free edges in a closed shell topology, where transverse bending is necessarily coupled to lateral stretching [15,16,17]. Consequently, the hybrid curvature-dilation mode might contribute with genuine transverse deflections to the shape fluctuations of spherical vesicles. The analytic problem was early addressed by Yeung and Evans [17], Faucon et al. [48] and Miao et al. [49], and recently revisited by Bivas [50]. In those exact theories of the spherical problem, when the analytic solutions are described in terms of the discrete spherical harmonics, the two curvature modes (pure bending plus hybrid) appear naturally coupled. In compatibility with the distribution of the normal modes in the Seifert's theory [26,27], in those exact theories, the time-dependent correlations of the flexural deformations of the composite membrane are obtained with a bimodal form as [17,49,50]:

$$\left\langle \zeta_{\mathbf{k}}(t)\zeta_{-\mathbf{k}}(0)\right\rangle = a_1(k)e^{-\gamma_1(k)t} + a_2(k)e^{-\gamma_2(k)t} \tag{10}$$

However, although a bimodal spectrum is predicted by these exact theories of the spherical vesicle dynamics, the analytic expressions of the respective amplitudes and frequencies are too much complicated and their implementation in fitting algorithms of the experimental data is not straightforward. Grounded on the bimodal hypothesis, a minimal approach to the fluctuation spectrum was proposed in Ref. [19] for lipid bilayers with the spherical geometry. Here, we develop the detailed theory that following the same perturbative approach as in ref. [19], specifically accounts for the basal curvature of the spherical object. An enhanced coupling is expected in curved

vesicles, resulting in a strong influence of the hybrid curvatures on the global shape fluctuations. However, for very large vesicles with $R \to \infty$, a behavior similar to the flat membrane should be recovered.

III. MATERIALS AND METHODS

III-1. Chemicals: 1,2-dimyristoyl-*sn*-glycero-3-phosphocholine (DMPC) was obtained as powder of 99% purity from Avanti Polar Lipids (Alabaster, AL). The lipid was stored at -20ºC and used as received, without further purification. Ultrapure deionized water was obtained from a Milli-Q source (resistivity higher than 18 MOhm × cm, organic matter content < 5 ppb). With LUV's, deuterated water from Sigma (standard grade, 99.98 atom% isotopic purity) was used in all experiments as a dispersion solvent.

III-2. Giant Unilamellar Vesicles (GUVs). GUVs were prepared by the electro-formation method invented by Angelova [51] using the optimised protocol described by Mathivet et al. [52]. The precursor lipid film is prepared as described above for preparing LUVs. DMPC GUVs in the fluid state were prepared inside the oven (at 45ºC), at a high temperature well above the melting temperature of the phospholipid (T_m = 23ºC).

III-3. Large Unilamellar Vesicles (LUVs). LUVs were prepared by the extrusion method using a commercial miniextruder (Liposofast, AVESTIN, Canada). To avoid possible differences between DLS and NSE experiments, we always used D_2O as the aqueous solvent (Sigma; 99.98 % isotopic purity). To prepare vesicles, the powder lipid is first dissolved in a chloroform/methanol mixture (2:1) using a test tube. Later, the solvent is slowly removed by evaporation in a dry nitrogen stream, yielding a homogenous lipid film consisting of multiple lamellae. The lipid film is then hydrated by pouring the aqueous phase into the tube. During the hydration phase (1h), the dispersion is frequently vortexed and maintained above the melting temperature of the

lipid (T_m = 23ºC for DMPC). Then, the lipid suspension is extruded through a polycarbonate filtering membrane (Whatman, Florham Park, NJ) with a defined pore size (200nm), producing unilamellar vesicles with a diameter near the pore size. Extrusion is performed inside an oven at a temperature fixed at least +10ºC above T_m,. Ten extrusion cycles ensure a homogeneous dispersion of LUVs with a constant size and low polydispersity [53]. The dispersion was then filtered through a 0.2-μm teflon filter and poured into quartz tubes. The concentration of the vesicle suspensions was fixed constant at 2mg/mL (final concentration), a value diluted enough to avoid interaction effects. For further details on the procedures, see Ref. [10].

III-4. Ultra-fast videomicroscopy-based flickering spectroscopy. Membrane fluctuations were tracked at the equatorial plane of GUVs made of DMPC. Experiments were performed at 30.0 ± 0.5 ºC. We used an inverted microscope working in the bright field mode (Nikon 80i) equipped with an ultrafast CMOS camera (Photron FastCAM SA3, 200 kfps max. rate, 1Mpixel; 8Mbytes RAM). Instantaneous fluctuations are decomposed as a discrete series of Fourier modes, $h(t) = \Sigma_l\, h_k(t) \exp(ik_l x)$, where $k_l = l/R$ is the equatorial projection of the fluctuation wavevector (R being the radius and l = 2, 3, 4, …∞ being the azimuthal number). The dynamics of the equatorial fluctuations is experimentally probed through the autocorrelation function defined as $G_q(t) = \langle \zeta_k(t-t') \zeta_k(t') \rangle$, where $\langle\ \rangle$ indicates time-average over the time series obtained from a given fluctuation sequence. Good statistics are achieved only if time averaging is performed over long time intervals (typically, 5s long at 20kHz sampling; $n \approx 10^5$ frames). The present ultrafast method is able to track fluctuations over very long periods of time, thus allowing a coherent detection of different components appearing correlated over very

different time scales. This technical goal was not achieved in previous flickering spectroscopy studies involving much slower videomicroscopy [34].

III-5. Dynamic Light Scattering (DLS). DLS measurements were carried out in the ILL Laboratory of the Partnership for Soft Condensed Matter (PSCM@ILL). Measurements have been performed using an ALV CGS-3 DLS/SLS Laser Light Scattering Goniometer System (ALV GmbH Langen, Germany). This instrument allows a simultaneous measurement of static and dynamic light scattering in an angular range from 25º up to 155º. It is equipped with a HeNe laser operating at a wavelength of 632.5 nm with a power of 22mW. An ALV / LSE-5004 Light Scattering Electronics is used together with an ALV-7004 fast multiple τ digital correlator. Scattering intensities are recorded via a pseudo-cross correlation setup, consisting of a fibre-optical detection unit with a fiber based beam splitter and 2 APD detectors. For DLS measurements, a small aliquot of the same vesicle suspension prepared for NSE experiments is diluted in D_2O (1:10 *v*/*v*). DLS (0.2mg/mL) and NSE (2mg/mL) experiments were indeed performed with the same vesicle suspension, running DLS immediately before starting the NSE experiment. The samples were poured into quartz cells (10mm O.D., Hellma). Then, they were placed in the measurement cell which was filled with decaline to match the refractive index of the quartz sample cells. Temperature inside this cell was measured by a Pt-100 sensor and kept constant at 30.0 ºC with a precision of ±0.1 degrees. The intensity correlation function $g^{(2)}(q,t)$ was measured as a function of the scattering wavevector q using the ALV-7004 hardware correlator. This function is related to the field autocorrelation function $g^{(1)}(q,t)$ through Siegert's relation:

$$g^{(2)}(q,t) = 1 + C\,|\,g^{(1)}(q,t)\,|^2 \qquad (11)$$

Here, C is an instrumental parameter. The field autocorrelation function is analyzed by CONTIN [54], an algorithm based on the inverse Laplace transform. Identical results are obtained by REPES [55]. No assumption about either the number of relaxation processes or the distribution shape is required in these methods. The autocorrelation functions $g^{(1)}(q,t)$ are described as a distribution of correlation times $G(\Gamma)$ centred at a given relaxation rate $\Gamma_T(q)$ and with bandwidth $\Delta\Gamma_T$ which is an accurate estimate of the standard deviation of the relaxation rates due to sample polydispersity.

III-6. Neutron Spin Echo (NSE).

The neutron scattering length for hydrogen and deuterium differs strongly. Therefore, the dynamic structure factor from sample hydrogen atoms can be experimentally accessed most directly by inelastic neutron scattering using a deuterated solvent to generate the necessary contrast. Because of its high energy resolution compared to other neutron scattering techniques, neutron spin echo (NSE) is optimally suited to probe over damped internal modes in fluctuating systems [56]. The reported NSE experiments were performed on the IN15 instrument at the ILL, Grenoble [57]. This instrument provides the longest Fourier times currently available worldwide at NSE instruments. The samples were filled into quartz cells (1mm thickness, Hellma). The instrument was equipped with a thermostatic holder for these cells and all measurements were performed at a temperature of 30.0±0.1ºC. A Fourier time ranging up to 207ns was explored at different q-values in the range from 0.184nm^{-1} up to 1.201nm^{-1}. To achieve this, measurements at wavelengths of λ = 12Å and 15Å had to be performed. The wavelength distribution in both cases had a FWHM of $\Delta\lambda/\lambda$ = 0.15. The experimental protocol follows our initial design proposed in Ref. [58], which is currently considered the standard method to measure membrane fluctuations in LUV systems [59,60].

IV. RESULTS AND DISCUSSION

IV-1. Shape fluctuations in bilayer vesicles

a) Spherical shells: Curvature-dilation coupling. Curved membranes entail deformation properties, which are fundamentally different from those with a planar geometry [30]. The deformation of curved sheets, usually referred to as shells, is entirely dominated by the curvature of the reference state. In this case, even for small deflections compared to the shell thickness ($\zeta < h$), the stretching that accompanies a bending deformation is a first-order effect [30,46]. The general linear theory of thin shells (with small thickness compared to the other dimensions, $h < R$) [46] assumes that any deflection occurred throughout the shell is completely defined by changes in curvature of the neutral surface, which is regarded as a planar body where the 3D-shell problem is projected [46]. In the spherical case, the linear theory establishes for the longitudinal strain [46]:

$$u_{ii}^{(sph)} = u_{ii}^{(pl)} + \frac{\zeta}{R} \tag{12}$$

where R is the spherical radius of curvature and $u_{ii}^{(pl)}$ the planar contribution from the in-plane deformations [46]. For a highly curved membrane ($R \to 0$), the dilational strain is strongly influenced by the normal deflection. However, in the limit of a planar membrane ($R \to \infty$), the second term in the right hand of Eq. 12 vanishes and the in-plane component $u_{ii}^{(pl)}$ must recover the expression in Eq. 5. Therefore, for a curved vesicle bilayer the generalized linear strain field in Eq. 12 might be re-written as:

$$u^{(sph)} = \frac{h}{2}\nabla^2\zeta + \frac{1}{R}\zeta \tag{13}$$

Using the spherical harmonics as a base to describe the membrane deformations, the condition $R^2\nabla^2\zeta_{lm} \approx l(l+1)\zeta_{lm}$ is fulfilled, so Eq. 13 predicts a ratio of the normal deflection to the dilation ultimately defined by the membrane thickness and the vesicle radius; for $kR > 1$, taking $k \approx l/R$, for the (linear) coupling factor one obtains:

$$\left(\frac{\delta\zeta}{\delta u}\right)_{sph} \approx \frac{R}{1+R/R_0} \tag{14}$$

with $R_0 = 2/hk^2$, a k-dependent characteristic radius which defines a crossover between two curvature regimes.

For small vesicles, with radius smaller than the characteristic value, $R < R_0$ (high-curvature regime), the second term in the denominator of Eq. 14 vanishes, so the shell-component becomes dominant with a coupling factor increasing with the vesicle radius, this is $(\delta\zeta/\delta u)_{R<R0} \approx R$. However, for large vesicles ($R > R_0$), the coupling factor becomes R-independent, converging to a constant value in the planar membrane limit, $(\delta\zeta/\delta u)_{R>R0} \approx R_0 = 2/hk^2$, the coupling factor that corresponds to the Helfrich's conjecture for the planar membrane [61].

b) Bimodal fluctuation spectrum. In the simplest approach, we will assume the influence of hybrid modes as a first-order perturbative contribution to the curvature motion. When the normal deflection is expanded in terms of the dilational strain, up to first order, $\zeta(u) = \zeta_0 + (\partial\zeta/\partial u)_0\, u + o(u^2)$ with $\zeta_0 = \zeta(u=0)$ being a pure bending deflection and $u = \delta A/A_0 = \delta\rho$ the dilational strain (which is equivalent to density-difference field in the Seifert formalism). Within this perturbative approach, the fluctuation spectrum of the spherical vesicle is expected with the bimodal form [19]:

$$\left\langle \zeta_k^2 \right\rangle \approx \left\langle \zeta_k^2 \right\rangle_0 + 2\left(\frac{\partial\zeta}{\partial u}\right)_{sph} \left\langle \zeta_k u_k \right\rangle_{hyb} \tag{15}$$

where $(\partial\zeta/\partial u)_{sph}$ stands for the linear value of the coupling factor given by Eq. 14. The zero-th order term $\langle\zeta_q^2\rangle_0$ represents the dominant component arising from pure bending modes and $\langle\zeta_q u_q\rangle_{hyb}$ the amplitude of the new hybrid component. For each mode, we consider approximate solutions as those obtained for pure bending and hybrid modes in

planar membranes. Substituting Eq. 14 in Eq. 15, taking Eqs. 2, 7 for the respective spectral amplitudes, one finds a general expression for the bimodal spectrum $P(k) = A\langle\zeta_k^2\rangle$ as:

$$P(k) \approx \frac{k_B T}{\sigma k^2 + \kappa k^4} + \frac{12R/h}{1 + R/R_0(k)} \frac{k_B T}{K k^2} \tag{16a}$$

which defines two different regimes depending on the vesicle size referred to the k-dependent characteristic size $R_0(k) = 2/hk^2$:

$$P(k) = \begin{cases} \dfrac{k_B T}{\sigma k^2 + \kappa k^4} + \dfrac{12R}{h} \dfrac{k_B T}{K k^2} & R < R_0 \\ \dfrac{k_B T}{\sigma k^2 + \kappa k^4} + \dfrac{24}{h^2} \dfrac{k_B T}{K k^4} & R > R_0 \end{cases} \tag{16b}$$

This spectrum is plot in Figure 1, which shows the renormalization effect of the hybrid mode over the bending-component of the membrane fluctuations. The first limit ($R < R_0$) corresponds to the bimodal regime considered in our previous publication [19] (see Eq. 16b; first equation). Thus, in small vesicles ($R < R_0$), the hybrid mode contribute to increase the amplitude of the high-k curvature fluctuations, which can be explained as an apparent softening characterized by a (R-dependent) effective bending modulus $\kappa_{curv}(R)/\kappa \approx 1 - 12(R/h)(\kappa q^2/K)$. Since $\kappa \sim h^2 K$ [47], the softening factor is expected to increase linearly with the vesicle radius as $\Delta\kappa(R)/\kappa = (\kappa - \kappa_{curv})/\kappa \sim R/R_0$, a direct consequence of the effective conversion of the bending energy into dilational in the curved vesicle.

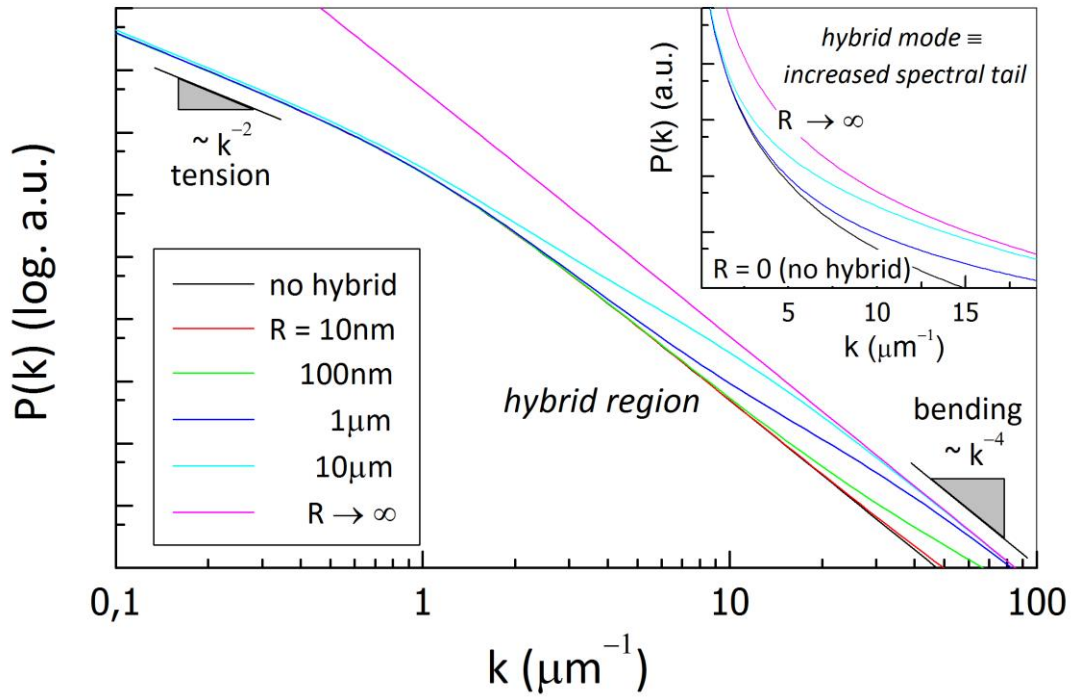

Figure 1. Theoretical prediction for the bimodal fluctuation spectra of vesicle membranes at different radius (taking variable R in Eqs. 16 with typical values: h = 2nm, $\sigma = 10^{-6}$ N/m, $\kappa = 20k_BT$ and K = 0.1N/m). The monomodal case (*no hybrid*) stands when the radius is set to zero in Eqs. 16. For finite radius, mode mixing occurs in the intermediate k-region, $k \approx k_C \approx (hK/12R\kappa)^{1/2}$, where the hybrid mode becomes energetically cheaper than the bending mode. Renormalized limiting behavior is recovered at low-k (tension like, $P(k) \sim k^{-2}$) and at high-k (bending-like, $P(k) \sim k^{-4}$) with an apparent lower bending rigidity accounting for effective softening due to hybrid modes (see main text for details). In the quasi-planar limit, $R \to \infty$, effectively softened bending-like behavior dominates, the bending constant taking a R-independent limiting value, $\kappa_{flat}/\kappa \approx 1-24\kappa/h^2K$ (see Eq. 16b at $R >> R_0$). **Inset)** Apparent softening mediated by hybrid modes in the spectral window relevant for flickering spectroscopy with giant vesicles. The larger the radius the higher the spectral tail, whose amplitude is defined by a lower effective bending rigidity ($\kappa_{curv}(R) < \kappa$), with the limit determined by the quasi-planar case ($\kappa_{flat} << \kappa$ at $R \to \infty$).

In this regime ($R < R_0$), a bimodal crossover is predicted between a low-k regime dominated by surface tension, $\sim k_BT/(\sigma k^2)$, and a soften high-k bending regime, $\sim k_BT/(\kappa_{cur}k^2)$, which is effectively governed by lateral dilations (the smaller K the higher the decrease $\Delta\kappa \sim K^{-1}$). For floppy vesicles ($\sigma \approx 0$), the transition of pure-bending motion to hybrid renormalization is predicted at a crossover wavevector weakly decreasing with the vesicle size as:

$$k_C(R) \approx \sqrt{\frac{hK}{12R\kappa}} \tag{17}$$

For very large vesicles ($R >> R_0$), hybrid modes also influence fluctuations as a softening contribution increasing the amplitude of the bending motions, $P_{bend} \approx k_BT/\kappa_{flat}k^4$. In this case, the effective bending modulus of the near-flat membrane becomes R-independent. Since $\kappa_{int} \approx h^2K/24$, it t could eventually take a vanishing value $\kappa_{flat}/\kappa \approx 1-24\kappa/h^2K \rightarrow 0$, an extreme behavior which determines a ceiling limit for the influence of hybrid modes with increasing radius. Indeed, if $R >> R_0$, one finds spectral tails characterized by very large fluctuations compatible with tension-dominated behavior ($P_{tens} \approx k_BT/\sigma k^2$ if $\kappa \rightarrow \kappa_{flat}$), whose amplitudes are no longer dependent on the vesicle radius. Indeed, the larger vesicles ($R >> R_0$) behave as quasi-planar bilayers with the maximum amount of membrane softening predicted by the detailed bilayer model of the planar bilayer assuming ideal relaxation of the dilational stresses between the two monolayers, *i.e.* $\kappa_{flat} \leq (h^2/24)K << \kappa_{curv}$.

Within our approach the bimodal spectrum takes a much simpler form than in the analytic treatments [48-50], thus allowing to fit the experimental data in a straightforward way. Furthermore, such a formulation allows an analytic discrimination of the different dynamical regimes and an adequate estimation of the range of applicability, with an emphasis on the dependence of the hybrid fluctuations on the vesicle radius. In the next subsections, evidence on the existence of hybrid modes in bilayer vesicles of different sizes is presented from different experimental approaches. Flickering spectroscopy (FS) was used to probe shape fluctuations in giant unilamellar vesicles (GUVs, $R \geq 3\mu m$). Complementary, using large unilamellar vesicles prepared with smaller radii by extrusion (LUVs, $0.2\mu m > R > 25nm$), the high-q fluctuation dynamics dominated by hybrid modes was probed by neutron spin echo (NSE). We

prepared vesicles made of 1,2-dimyristoyl-*sn*-glycero-3-phosphocholine (DMPC), a typical bilayer former with a moderate bending rigidity at the fluid state ($\kappa \approx 20 k_B T$ at $T > T_m \approx 23$ºC [31,42,43]). The combined data from the two methods provide a broad range of vesicle sizes sufficient to determine the functional dependence of the hybrid modes on the vesicle radius as predicted by the bimodal theory described here (in Eq. 16).

IV-2. Bimodal spectrum in giant vesicles: Dependence on vesicle radius

The existence of hybrid bending-dilational modes in the fluctuation spectrum of bilayer GUV's was evidenced in previous works dealing with the shape fluctuations measured at the equatorial plane [19,20,21]. In ref. [19], a significant contribution was detected in the high-*k*'s fluctuations of POPC vesicles, where curvature is high enough to privilege the hybrid mode over the pure bending motion. In that regime ($k > k_C \approx 5\mu m^{-1}$), enhanced equatorial fluctuations (with an amplitude well above the noise level) were detected exhibiting an algebraic decay $\langle h^2 \rangle \sim k_x^{-1}$, weaker than expected for pure bending modes ($\langle h^2 \rangle_{bend} \sim k_x^{-3}$), but compatible with hybrid behavior [19]. Here, we studied vesicles made of DMPC (T_m = 23ºC; $K \approx 0.1$N/m, $\kappa \approx 20 k_B T$ at 30ºC [47]), a saturated phospholipid stiffer than the monounsaturated homologue POPC (T_m = –2ºC; $K \approx 0.1$N/m, $\kappa \approx 10 k_B T$ at 25ºC [47]). Because of its intrinsically higher rigidity, the DMPC bilayers must hinder pure bending modes compared to hybrid motion, which should even dominate more than in POPC vesicles. Additionally, because their twin-tails symmetry, DMPC bilayers belong to the free-sliding category where no intermonolayer fingering is expected. Figure 2A shows the amplitude spectra of the equatorial fluctuations of three giant vesicles with a different radius. For these vesicles, only at low wavevectors ($k < k_C \approx 1\mu m^{-1}$), the experimental spectrum is well described

by the Helfrich expression. From the fits to Eq. (2) in this regime, one finds $\sigma = 10^{-6}$J/m^2 (±60% stand. dev.; N = 23) and $\kappa = 8.0\ 10^{-20}\text{J} \approx 20 k_B T$ (±15%), in good agreement with literature data for DMPC [31,42,43,47]. The high dispersion in the calculated surface tension is intrinsically natural as each vesicle is created with a different excess area, thus with different tension. At higher wavevectors ($k > k_C \approx 1\mu\text{m}^{-1}$), however, the tail of the experimental spectra clearly exceeds the Helfrich prediction, which decays much faster (see Fig. 2A). Consequently, the present experimental data evidence for DMPC weaker decays and larger fluctuations than expected for pure-bending modes, as previously reported for POPC [19]. Such an excess, calculated as the difference of the experimental to the Helfrich spectra ($\Delta P_x = P_{exp} - P_{Helf}$), is shown in Fig. 2B. Here, one observes a regular decay as $\Delta P_x \sim k_x^{-1}$, with the absolute values systematically larger with increasing radius. This contribution is not compatible with capillary-like behavior (also scaling as $\sim k_x^{-1}$), which might be dominant only at low wavevector, well below a critical value, $k_{cap} \approx (\sigma/\kappa)^{½} << 1\mu\text{m}^{-1}$. Tail fluctuations increase linearly with the radius of the vesicle (see Fig. 2C), a systematic behavior that assigns increasingly larger fluctuations to larger vesicles. These features are compatible with the presence of hybrid modes of fluctuation which become dominant at higher wavevectors and progressively influential for the larger vesicles (see Eq. 16).

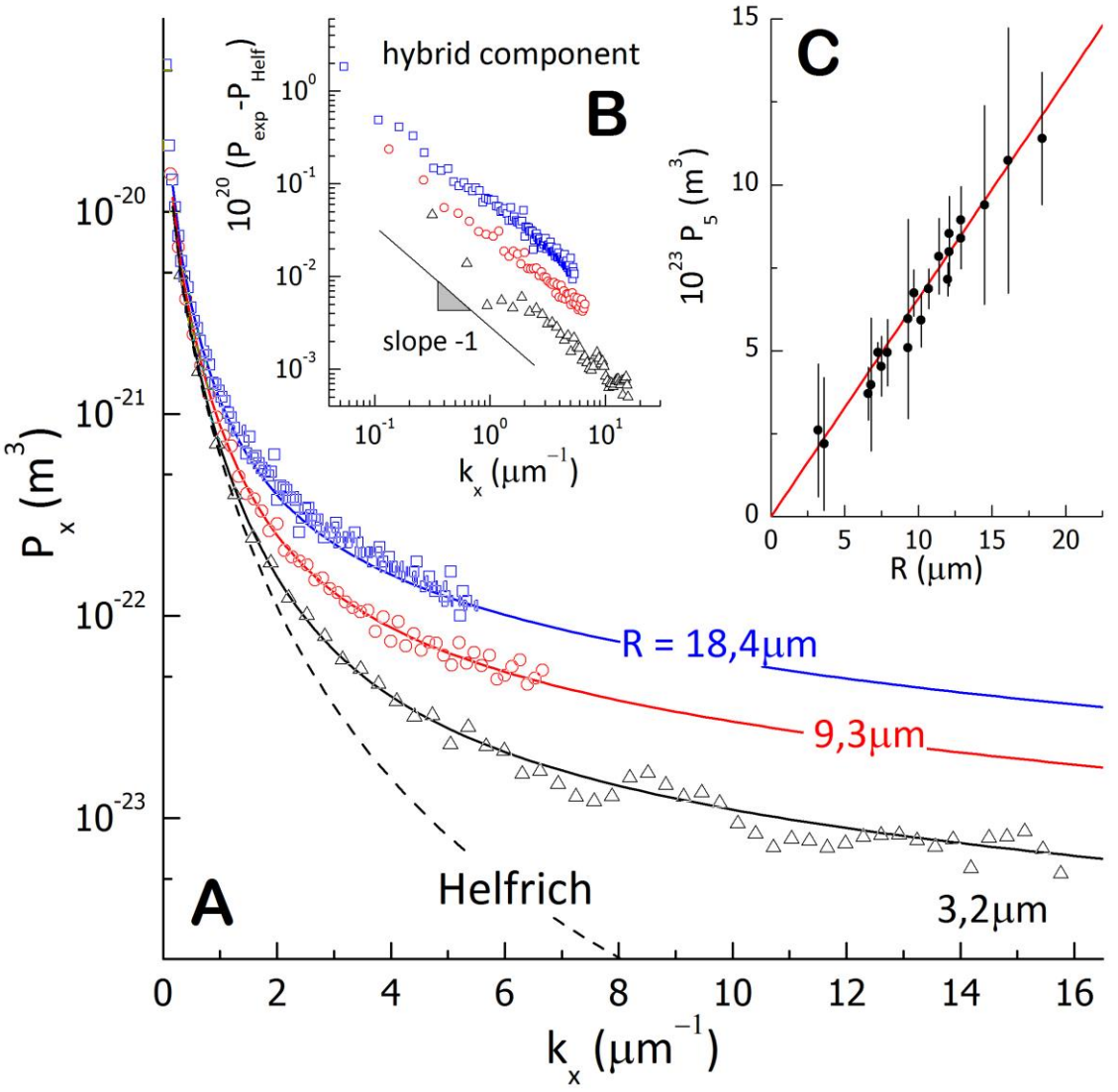

Figure 2. A) Experimental fluctuation spectra of DMPC GUV's recorded in the equatorial plane by ultra-fast flickering videomicroscopy (k_x is the equatorial projection of the 2D planar wavevector of the fluctuation modes, *i.e.* $k^2 = k_x^2 + k_y^2$). The different spectra correspond to three different vesicles with different sizes spanning the typical accessibility range. Whereas all the spectra overlap at the tension-like low-k region, higher tails are systematically observed with larger vesicles in the high-k, bending-like, spectral region. The straight lines correspond to the best fits to the bimodal spectra in Eq. 16a by fixing the radius R at the measured value (common fitting parameters for the considered population with N = 23 vesicles: h = 2nm (±15%, std. dev.), $\sigma = 10^{-6}$N/m (±60%), $\kappa = 8.2\ 10^{-20}$ J (±12%) = 20±2 k_BT, K = 0.085N/m (±15%). For comparison, the theoretical prediction from the monomodal tension/bending Helfrich spectrum is plotted as a dashed line ($\sigma = 2\ 10^{-7}$N/m, $\kappa = 20\ k_BT$ in Eq. 16a with $R = 0$). **B)** Difference between the experimental amplitudes and the monomodal Helfrich-spectrum ($\sigma = 2\ 10^{-7}$N/m, $\kappa = 20\ k_BT$). A R-increasing rest is identified with a $\sim k_x^{-1}$ decay typical of the hybrid mode (equatorial projection). **C)** Absolute spectral amplitude at the terminal bending tail (P_5 at $q_x = 5\mu m^{-1}$) for GUVs with different radius. The amplitudes follow a clear linear trend with increasing radius, $P \sim R$, as predicted by the bimodal spectrum in Eq. 16.

Therefore, hybrid bending-dilational modes provide a plausible scenario for explaining the enhanced amplitude of the high curvature modes. Since $K \approx 0.1$N/m, $\kappa \approx 20 k_B T$ for DMPC at 25ºC, for vesicles $R \approx 10\mu$m taking $h_{eff} \approx 2$nm [19] in Eq. 17, hybrid modes are hence expected to become dominant at $k > k_C \approx 3\mu m^{-1}$, just the high-$q$ regime of curvature fluctuations where the experimental spectral tails exceed the Helfrich spectrum. Indeed, fixing $h \approx h_{eff} = 2$nm and R at the observed value, all the experimental spectra, recorded for different radius, can be accurately fitted by the bimodal expression in Eq. 16 (case of $R < R_0 \approx 100\mu$m), for minimized values of the parameters $K = 0.085 \pm 0.010$N/m, $\kappa = (8.6 \pm 0.4)\ 10^{-20}$J $\approx (20\pm1) k_B T$, $\sigma = (1.0\pm0.6)\ 10^{-6}$ J/m^2 (the errors account for the standard deviations sampled over a population of $N = 23$ vesicles).

IV-3. Autocorrelation function. By taking advantage of time-resolved flickering spectroscopy, we probed the dynamics of the equatorial fluctuations in GUVs made of DMPC. Figure 3A shows typical height-to-height autocorrelation functions obtained from the same vesicle at different equatorial wavevectors, $k = l/R$ with ($l = 2, 3, 4, ... \infty$). In practice, no more than thirty modes can be analyzed, as no adequate statistics is reached in such faster modes. As expected, the higher the wavevector the faster the relaxation is. Whilst a monotonic exponential relaxation exists at low k's (see Fig. 3A for $l \leq 7$, $k \leq 1\mu m^{-1} << k_C$), a crossover to a bimodal behavior is observed for the higher wavevectors ($l > 7$). Similar bimodal behavior is detected in Fig. 3B where relaxation is plotted for a similar mode observed in vesicles with a different size. Obviously, the larger the vesicle the slower the relaxation of a given spherical harmonic; at constant l, the relaxation rate must decrease with R as $\gamma \sim k^\alpha \sim (l/R)^\alpha$ (with $\alpha = 3$ for pure-bending modes and $\alpha = 2$ for hybrid modes). The presence of a secondary mode at long times, becoming progressively important with increasing R, is clearly visible in this plot (see Fig. 3B).

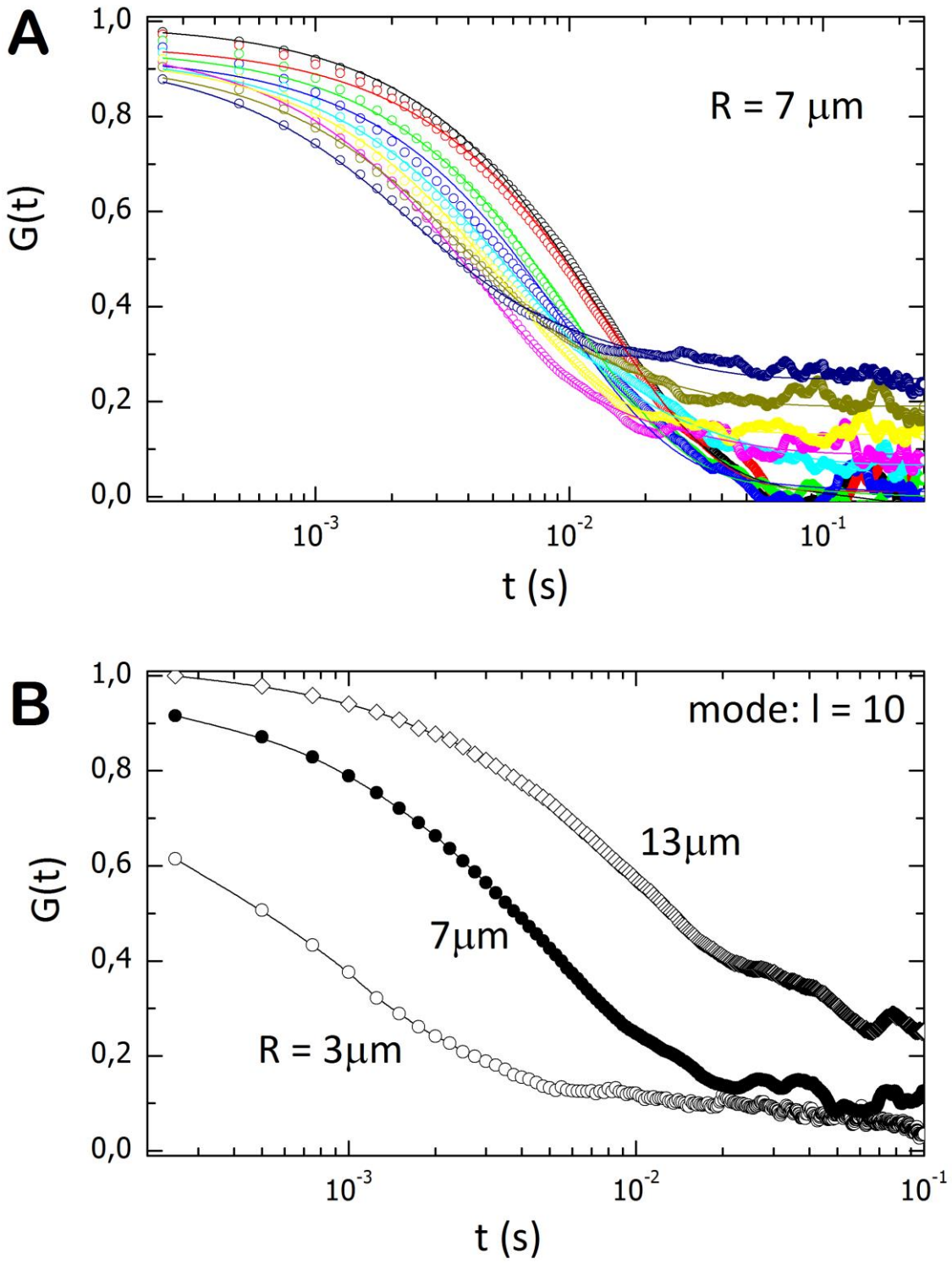

Figure 3. Height-to-height autocorrelation function in DMPC GUVs: **A)** Case of a given vesicle at different wavevectors (constant radius, R = 7mm); $k = l/R$: (○) l = 3; (○) l = 4; (○) l = 6; (○) l = 7; (○) l = 9; (○) l = 10; (○) l = 11; (○) l = 12; (○) l = 15. A secondary slow component corresponding to the hybrid mode clearly emerges with increasing k. **B)** The same mode (l = 10) in three different vesicles with different radius. In this case, the slower component appears progressively higher with increasing R.

To quantitatively analyze the relative influence of the two modes, fits of the experimental autocorrelation functions were performed to the bimodal expression in Eq. 10. Figure 4 shows the optimized values of the fitting parameters found for two vesicles with different sizes.

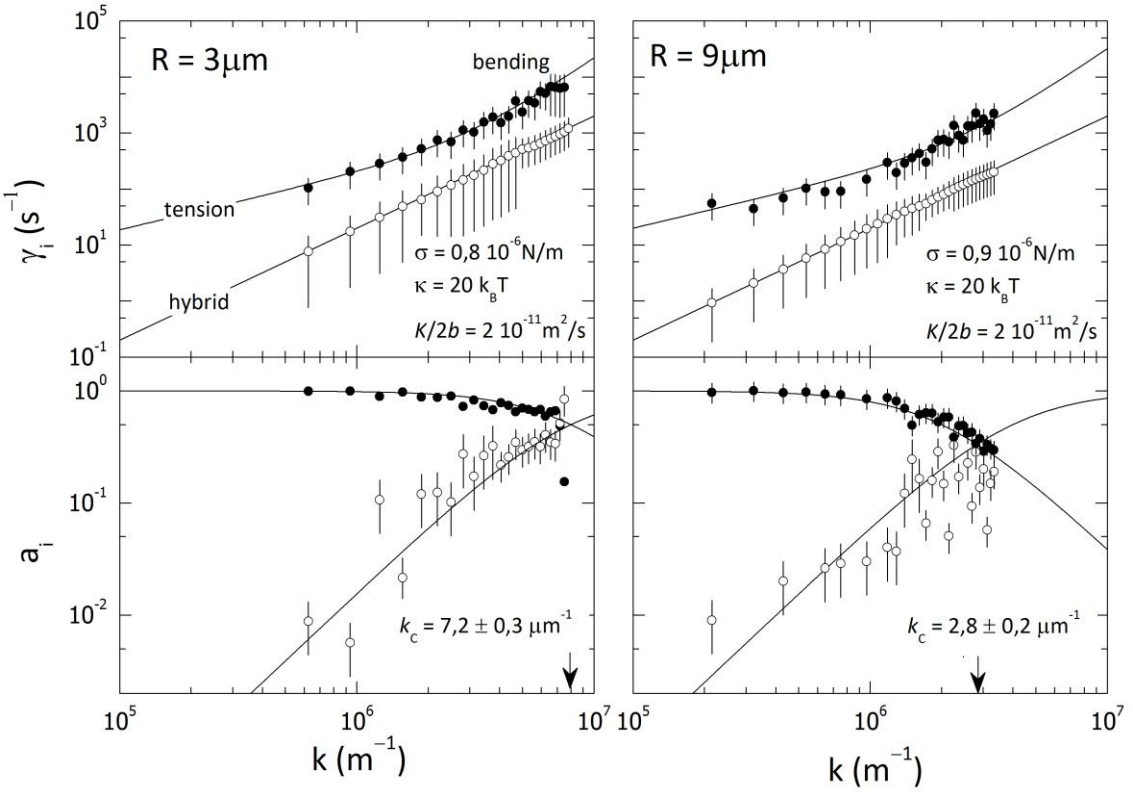

Figure 4. Bimodal analysis of the height-to-height autocorrelation functions for DMPC GUVs of two different sizes: (top panels) relaxation rates; (bottom panels) relative amplitudes. In both cases two modes are clearly identified, a slower one with dynamical characteristics as the hybrid mode ($\gamma_{hyb} \sim (K/2b)k^2$) and a faster one corresponding to a pure curvature motion which behaves bending-like at high-k ($\gamma_{bend} \sim \kappa k^3/4\eta$) but whose dispersion renormalizes to bending-like behavior at low-k ($\gamma_{tens} \sim \sigma k/4\eta$). The straight lines are theoretical predictions for the expected values of the constitutive parameters. The amplitudes are mutually normalized, the faster bending mode invariably decreasing at the expense of the hybrid mode which become dominant at high-k. The straight lines in the bottom panels corresponds to the best fits of the mode amplitudes to the theoretical expression in Eq. 18. The crossover wavevector at which both amplitudes equal (k_C, marked with an arrow) varies with the vesicle radius: the larger the vesicle, the lower k_C, as expected from Eqs. 17-18.

On the basis of the bimodal model, the two relaxation rates can be easily unfolded (see Fig. 4; top panels) as the decay rates of two separated exponentials with variable

amplitudes (see Fig. 4; bottom), whose sum is assumed to be mutually normalized ($a_1 + a_2 = 1$). In the studied range, the faster mode is found systematically dominant (with the higher amplitude, $a_1 > a_2$). The slower mode is found with a residual amplitude ($a_2 < 0.5$), systematically increasing with the wavevector although affected by a large error. The decay rate of the faster mode display rescaling behavior ($\gamma_1 \sim k^\alpha$ with $\alpha = 1–3$), which it can be rationalized as a mixing of a tension dominated regime at low wavevector ($\gamma_1 \approx \sigma k/4\eta$ at $k < 1\mu m^{-1}$) plus a renormalized pure-bending behavior at high k's ($\gamma_1 \approx \kappa k^3/4\eta$ at $k > 1\mu m^{-1}$). Assuming a dissipation governed by bulk friction (the viscosity of the water medium, η = 1cP), the relaxation rates of the faster tension/bending mode can be described by Eq. 4, by taking reasonable values of the corresponding elastic moduli ($\sigma \approx 10^{-6}$N/m, $\kappa \approx 20 k_B T$), in close agreement with the static values obtained from the time-averaged fluctuation spectra. Furthermore, the relaxation rates of the slower mode systematically scale as $\gamma_2 \sim k^2$, a dispersion law compatible with hybrid modes ($\gamma_2 \approx (K/2b)k^2$, see Eq. 8). By fitting to the experimental rates, a value of the numeric prefactor $K/2b$ = (2.0±0.8) 10^{-11} m^2/s is found as a statistically representative average over all the vesicles studied (N = 21). Because a value K = 0.085 ± 0.010N/m was obtained from the static spectra, the intermonolayer friction coefficient is deduced with a value b = (2.1±1.1) 10^9 N s/m^3, in quantitative agreement with previous FS data on GUVs of similar phospholipids [19,21], and estimations obtained in tether pulling experiments [62] and from measurements of the lateral diffusivity of fluorescent probes [63]. Very similar rates are found with different vesicles (see Fig. 4; top), a behavior compatible with the hypothesized bimodal scenario where each mode (pure-bending and hybrid), relax with a separated frequency governed by the ratio of the corresponding restoring forces to viscous dissipation, which are independent of the size of the vesicle. Different is the case of amplitudes, however,

whose *k*-dependence is found linearly dependent of the radius of the vesicle (see Fig. 4; down panels). Whereas a minor hybrid contribution subsidiary of the main bending mode is detected in the smaller vesicles (see Fig. 4A), a progressive higher influence is observed with increasing radius (see Fig. 4B). Above crossover, the hybrid mode is prevalent with a dominance shifting to lower wavevectors with increasing the radius of the vesicle. Here, we found again size-dependent behavior, a consequence of the bimodal behavior described by Eqs. 10. With GUVs, assuming a size-regime with $R < R_0$ ($\approx 100\mu m$), for $\sigma << \kappa k^2$, Eq. 16 predicts the relative amplitudes respectively varying as:

$$a_{bend} \approx \frac{1}{1+\left(k/k_C\right)^2} \quad a_{hyb} \approx \frac{1}{1+\left(k_C/k\right)^2} \tag{18}$$

which are mutually normalized and show a crossover at the critical wavevector k_C, given by Eq. 17 (expected to decrease with radius as $k_C \sim 1/\sqrt{R}$).

We show in Fig. 4 (bottom panels) the best fits of the experimental amplitudes with the theoretical expressions in Eq. 18. Good quantitative agreement is found between experiment and the model, which accurately describes the crossover point displayed by the experimental data (see Sec. IV-6 for a further discussion). In Fig. 4, we clearly observed the calculated crossover wavevectors k_C to decrease with increasing radius. These absolute values measured with GUVs in the micrometer size domain will be discussed in Section IV-6 in conjunction with high-*k* data measured with nanometer sized vesicles (LUVs) in the NSE window.

IV-4. Dependence of the fluctuation amplitudes on vesicle radius

The theoretical expression of the bimodal spectrum derived in this study (see Eq. 16), predicts a progressive dominance of the hybrid mode at high wavevectors (see Fig. 4B). However, two different regimes are predicted depending on the vesicle radius. For small

vesicles ($R << R_0$), hybrid modes are expected with an increasing amplitude with increasing radius. However, for very large vesicles ($R >> R_0$), the relative amplitude of the hybrid contribution reaches a saturation level given by the constant ratio between bending and compression stiffness, this is $a_{hyb}/a_{bend} \approx 24\kappa/Kh^2 \approx \kappa/\kappa_{int}$. The transfer function is given by $\Phi(R) = 12(R/h)/(1+R/R_0)$, which describes how far the hybrid modes contribute to the spectrum depending on the radius of the vesicle. Since the characteristic radius depends on the probed wavevector, for curvature modes in the FS window ($k \approx 1\mu m^{-1}$), one expects planar membrane behavior with vesicles sizes well above $R_0 = 2/hk^2 \approx 10^3$ μm. For GUVs one has typically $R < R_0$, thus we expect a linear increase of the relative contribution of the hybrid mode, this is $\Phi(R < R_0) \approx 12(R/h)$. In Figure 5 we show the relative amplitudes of the hybrid mode as obtained from the bimodal diagrams in Fig. 4B for vesicles with different radius.

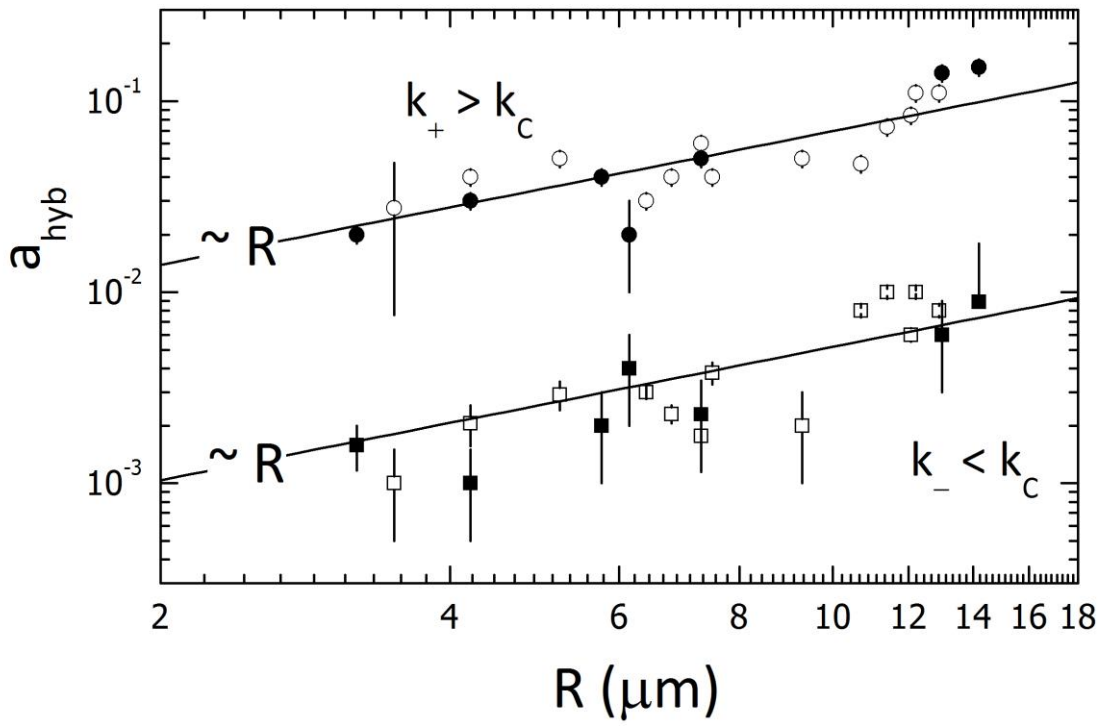

Figure 5. Linear dependence of the relative hybrid amplitudes on the vesicle radius. Different vesicles in two different samples are considered. As expected, the linear dependence $a_{hyb} \sim R$ is preserved below ($k_- = 1\mu m^{-1} < k_C$) and above ($k_+ = 10\mu m^{-1} > k_C$) the crossover wavevector, k_C.

A linear increase with radius is observed independently of the dynamic regime considered (below or above k_C), a behavior compatible with the trend expected from the theoretical spectrum proposed in Eq. 16 ($R < R_0$).

IV-5. High-*q* fluctuations: Bimodal theory of scattering and NSE experiments

a) Bimodal dynamic structure factor. The intermediate scattering function $S(q,t)$ contains the relevant information about the scattering length density fluctuations in a scattering system. It is the Fourier transform of the dynamic structure factor which measures the frequency spectrum of the thermally excited fluctuations as a function of transfer wavenumber [64,65]. In a complete theory of scattering by fluctuating vesicles, translational diffusion must be considered as the main contribution to the dynamic structure factor. Then, bending modes appear as a series of internal modes accounting for the shape fluctuations [64]. In the classical Milner-Safran (MS) theory of scattering by suspensions of spherical vesicles, the corresponding intermediate scattering function is written as a function of the magnitude of the 3D-scattering vector q as [7]:

$$S(q,t) = e^{-\Gamma_T t}\left[A_T(q) + A_{int}(q) S_{int}(q,t)\right] \tag{19}$$

with Γ_T being the diffusive rate of the translational motion:

$$\Gamma_T = D_T q^2 \tag{20}$$

where D_T is a translational diffusion coefficient given by the Stokes-Einstein formula for the sphere of radius R:

$$D_T = \frac{k_B T}{6\pi\eta R} \tag{21}$$

To describe the scattering from the internal modes of fluctuation of the flexible spherical membrane, the MS theory considers bending modes as discrete spherical

harmonics and couples their relaxation dynamics with the effective viscous friction exerted by the bulk solvent [6]. On the one hand, $A_T(q)$ accounts for the relative amplitude of the translational mode, which is proportional to the size of the diffusing object. Particularly, in the MS treatment, the amplitude of the translation component is determined by the q-dependence of the spherical structure factor [7]:

$$A_T\left(q;R\right) = 4\pi\left[\, j_0\left(qR\right)\right]^2 \tag{22}$$

which is defined by the modulus of the zero-th order spherical Bessel function.

On the other hand, $A_{int}(q)$ accounts for the relative contributions of all the internal modes of fluctuation, *i.e.* the succession of spherical harmonics whose effective time dependence is given by the dynamic function $A_{int}(q)\, S_{int}(q,t) = \sum_l A_l\, S_l(q,t)$ (with l = 2, 3, …∞ being the azimuthal number defining the wavelength of the internal fluctuation) [7]. Furthermore, due to the intrinsic normalization of the spin-echo experiment, the two relative amplitudes in Eq. (19) are defined in a way such that they are coupled and their sum is fixed to 1 [7,64], *i.e.* $A_{int} = 1 - A_T$. In the ZG model [35,36], the discrete succession of normal modes of fluctuation is approached in the continuous Fourier approximation, which can be easily integrated following the general formalism reproduced in the Appendix. For bending modes [35,36], the ZG theory predicts a stretched exponential decay of the dynamic structure factor [see Eqs. A17-18], which arises from a collective subdiffusive dynamics of the bending modes of the membrane [35,36]. Such an anomalous fluctuation diffusivity is easily understood when the two-point correlations are calculated for the membrane modes governed by bending elasticity (see refs. [35,36,66] and the calculations reproduced therein in the Appendix). For pure bending modes one has $\langle h^2\rangle_{bend} = k_BT/\kappa k^4$ and $\gamma_{bend} = (\kappa/4\eta)k^3$, so the ZG formalism predicts in that case:

$$S(q,t) = e^{-\Gamma_T t}\left[A_T + (1-A_T)\,S_{bend}(q,t)\right] \tag{23}$$

with $S_{bend}(q, t)$ given as in Eqs. A17-A18 in the Appendix; the specific ZG expression for the dynamic structure factor of the bending fluctuations:

$$S_{bend}(q,t) \approx \exp\left[-(\Gamma_B t)^{2/3}\right] \tag{24}$$

with a k^3-dependent decay rate:

$$\Gamma_B \approx 0.025\left(\frac{k_B T}{\kappa}\right)^{1/2}\frac{k_B T}{\eta}q^3 \tag{25}$$

If hybrid modes were also present, then, a bimodal expression is expected in Eq. 19 for the scattering contribution from the internal modes of fluctuation; consequently, Eq. 23 must rewrite as:

$$S(q,t) = e^{-\Gamma_T t}\left\{A_T + (1-A_T)\left[a_{bend}S_{bend}(q,t) + a_{hyb}S_{hyb}(q,t)\right]\right\} \tag{26}$$

which is the general expression proposed in ref. [59] to explain NSE data in vesicle systems undergoing shape fluctuations with the twofold nature, pure-bending and hybrid. A specific expression for the hybrid structure factor will be developed in the next subsection.

b) ZG formalism for hybrid fluctuations. In the case of fluctuating membranes, NSE signals contain information on the hydrodynamic correlations between different points in the membrane. For the membrane fluctuations, ZG developed a formalism which connected the dynamic structure factor with the two-point correlations [35,36,66]. Following the generalization of the ZG formalism described in the Appendix, specific expressions for the dynamic structure factor can be obtained for the membrane fluctuations driven by hybrid modes. In such case, looking at Eq. 8 and Eq. 9, one expects $\langle h_q^2\rangle_{hyb} \approx 12(R/h)\ k_BT/Kq^2$ and $\gamma_{hyb} \approx (K/2b)q^2$, so to calculate the dynamic

correlations between hybrid fluctuations, the relevant variable change in Eq. A10 is now $z = \xi_{hyb}\, q$, with a characteristic length with the form $\xi_{hyb} = (Kt/2b)^{1/2}$ determined by the compression modulus K and the intermonolayer friction coefficient. Consequently, for hybrid modes, the integral in Eq. A10 for the corresponding dynamic correlator can be written as follows:

$$\phi\left(r-r',t\right)=\frac{1}{2\pi^2}\left[12\frac{R}{h}\frac{k_BT}{K}t^0\right]F_{hyb}\left[\left(r-r'\right)/\xi_{hyb}\left(t\right)\right] \tag{27}$$

where the remnant $\phi \sim t^0$ dependence arises from the scaling symmetry between the mode energy $E_{hyb} \approx Kq^2$ and its corresponding dissipation which is characterized by a proportional damping coefficient $\gamma_{hyb} \approx (K/2b)q^2 \approx E_{hyb}/2b$. In the case of hybrid modes, the specific scaling function takes the form:

$$F_{hyb}\left[u\left(t\right)\right]=\int_0^\infty\int_0^\infty e^{iu(t)z}\,\frac{1-e^{-z^2}}{z^2}\,d^2z \tag{28}$$

in function of the dimensionless distance:

$$u\left(t\right)=\frac{r-r'}{\xi_{hyb}\left(t\right)}=\frac{r-r'}{\left(Kt/2b\right)^{1/2}} \tag{29}$$

At short distances ($u \to 0$), the complex kernel $e^{iu(t)z} \to 1$, so the integral in Eq. (28) can be approximated as $F_{hyb}(u) \approx 1 + o(u^2) \sim t^0$. Therefore, up to same order of approximation than for bending modes in the ZG treatment [36], a stationary trajectory independent of the frictional losses is predicted here for hybrid modes; this is:

$$\left\langle \Delta h^2\left(t\right)\right\rangle_{hyb} \approx \phi\left(u\to 0,t\right)\approx 0.61\frac{R}{h}\frac{k_BT}{K}t^0 \tag{30}$$

Surprisingly, if hybrid modes dominate in bilayer membranes, Eq. 30 predicts a very fast approach to a stationary trajectory compatible with the saturation value of the hybrid amplitudes. For the hybrid modes in the spherical shell, the saturation limit is

given by the sum of amplitudes extended over all the fluctuation modes $\langle \Delta h^2(t\to\infty)\rangle_{hyb} \approx A^{-1} \sum_k (12R/h)(k_BT/Kk^2)$, where the sum of modes is extended from $l = 2$ (the largest one) up to $l \to \infty$. Assuming a spherical area $A = 4\pi R^2$, since $k = l/R$, one finds $\langle \Delta h^2(t\to\infty)\rangle_{hyb} \approx (12/4\pi)\,(R/h)\,(k_BT/K) \sum_{l\geq 2} l^{-2}$, where the series converges to the exact value $\sum_{l\geq 2} l^{-2} = (\pi^2/6) - 1 \approx 0.64$ (Basel problem). Consequently, for hybrid modes, one might find a RMS saturation limit at $\langle \Delta h^2(t\to\infty)\rangle_{hyb} \approx 0.61(R/h)(k_BT/K)$, just at the stationary value predicted by Eq. 30.

Therefore, keeping the same degree of approximation (zero-th order; $F_{hyb}(u) \sim t^0$ at $u \to 0$) than the one considered in the original treatment for bending modes in rigid membranes ($F_{bend}(u \to 0) \sim t^0$ at $\kappa >> k_BT$), when the general ZG formalism is particularized to hybrid modes in the rigid membrane ($K \to \infty$), a time-independent term must be considered when looking at the specific dynamic structure factor of the membrane fluctuations. Therefore, substituting Eq. 30 into Eq. A4, one finds a Gaussian profile which defines a static structure factor of the hybrid membrane fluctuations dominated by compression elasticity:

$$S_{hyb}(q,t)/S(q,0) \approx \exp\left(-0.3\frac{R}{h}\frac{k_BT}{K}q^2t^0\right) \tag{31}$$

The present analytic result depicts hybrid fluctuations as a highly dissipative mode of curvature motion ($\gamma_{hyb}/E_{hyb} \approx 2b$), with a relative overdamping higher than the usual bending modes ($\gamma_{bend}/E_{bend} \approx 4\eta q << \gamma_{hyb}/E_{hyb}$), thus exhibiting a much higher sub-diffusivity $\langle \Delta h^2(t)\rangle_{hyb} \sim t^0$, which is responsible for a zero-th order time-independent dynamic structure factor. Such a conclusion is identical to that previously reached by Watson and Brown through of a qualitative argument [28]. On the basis of the bimodal scenario (pure bending/hybrid) depicted by Seifert [26,27], those authors argue about the complete relaxation of the hybrid mode on the NSE window ($\gamma_{hyb} \approx Kq^2/2b <<$

$1/\tau_{NSE}$). Following those authors, because the dynamic intermediate scattering function measured in the experiment is determined by the time-dependent portion of relaxation, the already relaxed contribution from hybrid modes is expected to contribute only with an additive constant [28]. It is worthy notice that in the present formulation, the considered bimodal ZG formalism is zero-th order with respect to the characteristic distance u ($\sim (r-r')/\xi \rightarrow 0$). This restrictive condition determines the range of validity of the above approximation, which is strictly restricted to the asymptotic limit determined by the large characteristic lengths expected for the ideally rigid membrane (only if κ, $K \rightarrow \infty$ then $\xi_{bend}, \xi_{hyb} \rightarrow \infty$, so $u_{bend}, u_{hyb} \rightarrow 0$). At moderate rigidity not only higher order contributions ($\sim u^2$) but also intermodal crossed terms could eventually influence the time dependence of the dynamic propagator, and consequently modify the sub-diffusive character of the expected relaxation with stronger time-dependent fluctuations. In the opposite limit of very floppy/soft membranes (κ, $K \rightarrow 0$), a free-diffusion behavior is expected, a dynamical feature compatible with single exponential relaxation, as quoted experimentally in strongly fluctuating membranes [31,37-39].

c) NSE-data fitting. In the section above we have analytically demonstrated that no time-dependent contribution is expected from hybrid modes in the short lengths probed by NSE (if $u \rightarrow 0$ then $S_{hyb}(q, t) \sim t^0 \approx$ constant; see Eq. (31)). Consequently, at the same degree of approximation than in the original ZG theory, the bimodal expression in Eq. 26 for the NSE intermediate scattering function should be expected with the form:

$$S(q,t) \approx e^{-\Gamma_T t}\left\{A_T + (1-A_T)\left[a_{bend}\, exp\left[-(\Gamma_B t)^{2/3}\right] + a_{hyb}\right]\right\} \qquad (32)$$

with the translational amplitude fixed at the value given by Eq. 22 and the decay rate of the pure bending term given by Eq. 25.

Using the (zero-th order) bimodal structure factor in Eq. 32 to account for the two internal fluctuation modes (bending/hybrid), the experimental NSE intermediate relaxation functions can be rationalized as follows. Once the vesicle radius is known (by DLS), the characteristics of the translational term are absolutely determined (Γ_T and A_T). Afterwards, normalization imposes the absolute contribution of the two internal modes, *i.e.* $A_{int} = 1 - A_T$. Then, since two different internal modes are assumed to contribute to scattering, their relative contributions must be mutually normalized. In the present bimodal case, the respective pure- and hybrid- amplitudes might verify, $a_{bend} + a_{hyb} \equiv 1$. In practice, to fit NSE profiles to Eq. 32, both Γ_T and A_T are fixed at the expected values. To minimize cross-correlations between the fitting parameters, the relaxation rates of the bending term are assumed with the $\Gamma_B \sim q^3$ dispersion. Their absolute values are fixed predictions from Eq. 25 for the expected value of the bending modulus ($\kappa = 20 k_B T$ for DMPC at 30ºC). Then, a multidimensional fit is performed to search for the optimal combination of amplitudes (a_{bend}, a_{hyb}) that best describe the complete set of experimental data measured at different wavenumbers. Let's notice that the time-independent constant term considered in Eq. 32 for the hybrid contribution, $S_{hyb}(t) \sim 1$, assumes no mode relaxation ($\gamma_{hyb} << 1/\tau_{NSE}$), a dynamic behavior compatible with the no-time dependence of the correlations in the rigid membrane ($\phi_{hyb} \sim t^0$ if $K \to \infty$). In the opposite limit ($K \to 0$), however, a single exponential behavior should be expected, $S_{hyb}(t) \sim \exp(-\Gamma_{hyb} t)$, similarly to bending fluctuations in soft membranes [31,37-39]. This limiting behavior will be also considered in discussing the bimodal fits to experimental NSE data (see Supplementary Material).

d) NSE experiments with DMPC vesicles of variable radius: high-q crossover. We prepared LUV's of different radius by extrusion through membranes with a variable

pore size. Four samples with different nominal vesicle radius in the range R = 25-200nm were considered in this NSE study. Immediately prior to each NSE run with a given sample, the average vesicle size was in situ determined by DLS performed in the same sample (see results and data analysis in SM). Once the experimental distributions of DLS relaxation times were obtained, an average vesicle radius was determined by assuming diffusional translation behavior; from Eq. 20-21, one gets R ($\pm\sigma_R$), the standard deviation σ_R being estimated as size polydispersity causes significant broadening on the experimental distribution of the translational times (see refs. [31,**¡Error! Marcador no definido.**,43] for details). Figure 6 shows the complete experimental dataset obtained with the four DMPC samples containing vesicles of different radius. The raw NSE data are plotted in the top panel of Fig. 6. The translational contribution was unfolded by dividing the raw data by the translational relaxation term, $S_T(q,t) = \exp(-D_T q^2 t)$ (with D_T calculated from the Stokes-Einstein formula (Eq. 21) for the different vesicle radii). The bare contribution from the shape fluctuations $S(q,t)/S_T(q,t)$ is shown in the bottom panels in Fig. 6. The larger the vesicles the slower the translational relaxation, whose relative contribution to scattering appears progressively unrelaxed with increasing radius. Conversely, with the smaller vesicles, translational effects become progressively important with increasing q, thus making differences between the different cases to emerge when the translational component is conveniently unfolded (see Fig. 6B). Following the procedure described in Sec. IV-3.b, the remaining data $S(q,t)$ were fitted to Eq. 32. Taking the values of R obtained from DLS and $\kappa = 20 k_B T$, considering only the two amplitudes a_{bend} and a_{hyb} as fitting parameters, the bimodal model in Eq. 32 is able to describe the complete NSE dataset (see Fig. 6B) with the translational amplitudes A_T fixed at the value expected from Eq. 22 for each given radius.

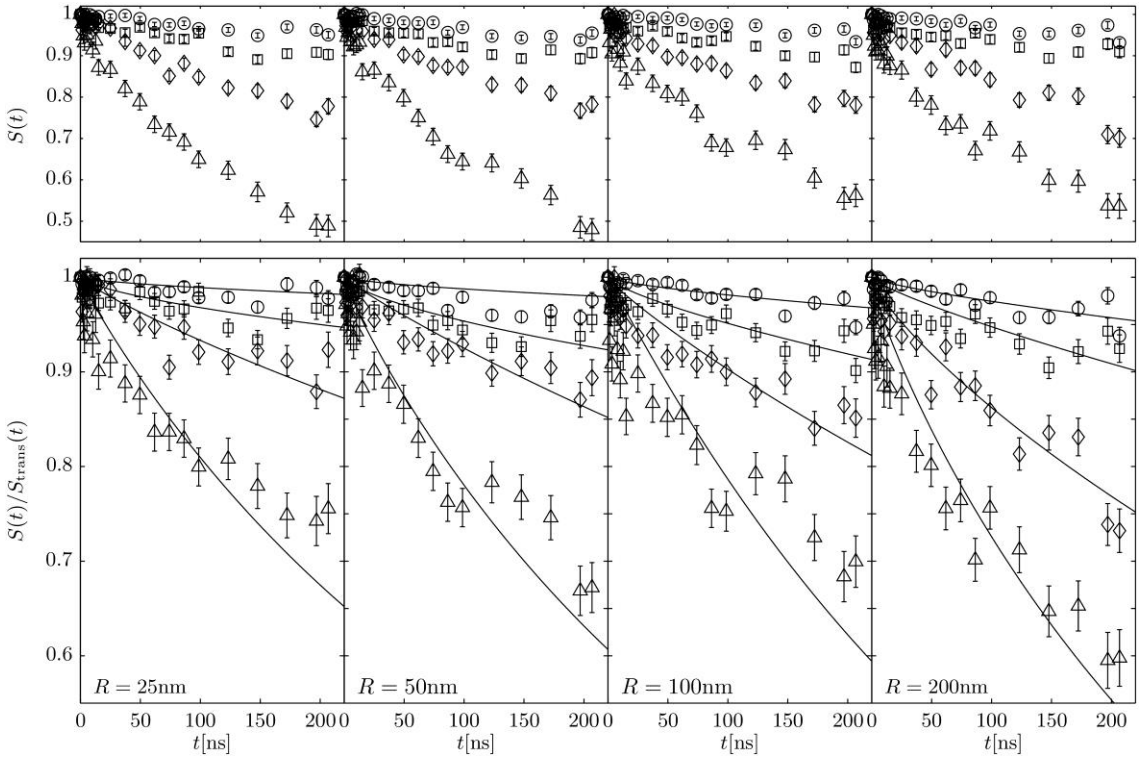

Figure 6. Analysis of the NSE intermediate functions obtained for suspensions of DMPC vesicles with different radius, R (the symbols represents different NSE wavenaumbers: q = 0.282nm^{-1} (○); 0.454nm^{-1} (□); 0.723nm^{-1} (△); 0.913nm^{-1} (▽): (Top panels), crude data; (Bottom panels), data reduced with the translational component, $S_T(q) = \exp(-D_T q^2 t)$ with D_T fixed in the value obtained from DLS. The straight lines correspond to the best fits to Eq. 32 (see Suppl. Material for a detailed discussion).

Figure 7 shows the fitted values of the two amplitudes as a function of the NSE wavenumber. Because experimental data are normalized, *i.e.* $S(q, 0) = 1$, the sum of both amplitudes is expected to be close to unity. Despite their treatment as independent fitting parameters, their sums show values systematically close to unity ($a_{bend} + a_{hyb} \approx 1$; see Fig. 7; bottom panel), a proof of likelihood of the bimodal model. In all cases studied, a systematic decrease of the pure-bending amplitude is observed in favor of the hybrid contribution, which becomes dominant with increasing q. Indeed, the high curvatures involved at high-q are expected to be dominated by dilational effects of stress relaxation [15]; in this regime, $q > 0.05$ Å^{-1}, the fluctuation wavelength becomes similar to the thickness dimensions, $h \approx \lambda < 12$nm, so following Eq. 14, $\delta\zeta/\delta u \approx R_0 \approx h$,

large longitudinal dilations are expected in this regime from small fluctuations even of the order of the membrane height, $\delta u \approx \delta\zeta/h$.

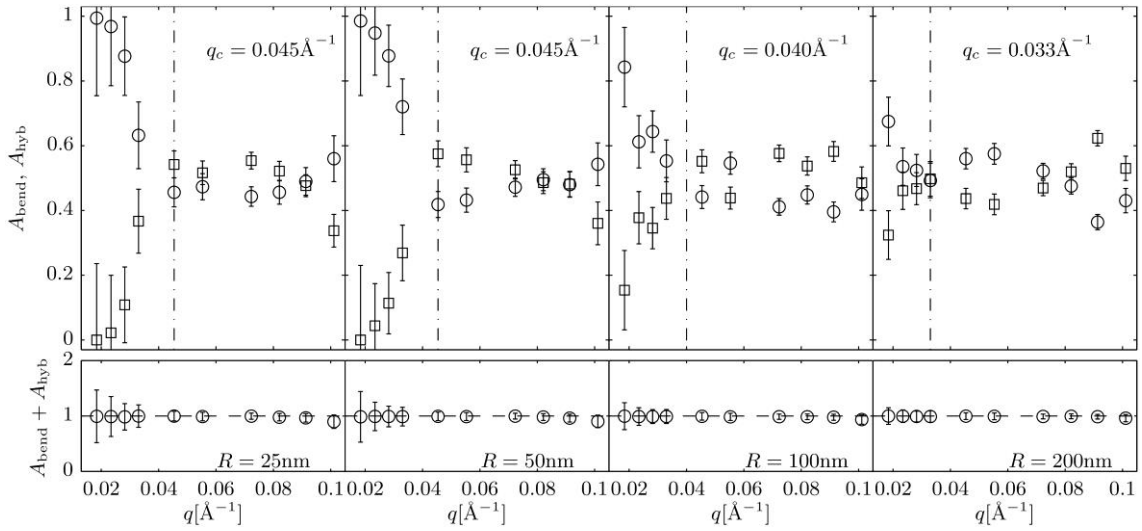

Figure 7. Top) Bimodal amplitudes inferred from the experimental NSE intermediate functions fitted to Eq. 32. Vertical lines mark crossover wavenumbers, q_C, estimated as the approximate first q-value where $A_{bend} \approx A_{bend} \approx 0.5$. **Bottom)** Proof of normalization: the two modes are obtained mutually normalized, *i.e.* $A_{bend} + A_{bend} \approx 1$, within the experimental uncertainty.

At a given q, each amplitude represents the relative amount of scattering by two different shape fluctuations with the same geometry but different class of internal motion (equal shape but different nature). At low q, scattering by bending modes systematically dominates over weaker hybrid motions ($a_{bend} >> a_{hyb}$), as expected. With increasing q, a progressive exchange is observed until reaching crossover at q_C when $a_{bend} \approx a_{hyb} \approx 0.5$. However, no further loss of the dominance of bending modes at the expense of hybrid motions is detected at higher q's, differently to the theoretical expectation (see Eq. 18; $a_{bend} \approx 0$ and $a_{hyb} \approx 1$ at $q > q_C$). An alternative analysis (see Fig. SM3), based on a time-dependent hybrid contribution with a single-exponential decay ($K \rightarrow 0$ limit; see discussion in Sect. IV-4b), provides better quantitative agreement with the bimodal prediction given by Eq. 18 (see SM; Fig. SM4b). Although

only a graphical estimate of q_C is possible from the amplitude data in Fig. 7A for the time-independent hybrid contribution, a semi-quantitative agreement is found with the crossover wavenumbers calculated from the more accurate data obtained when a time-dependent profile is assumed for the hybrid mode (see Fig. SM4). Anyway, similar mode exchange is likely described by the two methods, which account for the progressive dominance of the hybrid mode with increasing radius (see Fig. 7 and Fig. SM4).

IV-6. Crossover regime at different vesicle sizes

From these results, the bimodal character of the shape fluctuations in bilayer vesicles was clearly demonstrated. Upon a strong change of the membrane shape, if the constituting monolayers are locally deformable but their edges are closed, the corresponding global change of curvature in the bilayer occurs followed by a reorganization of the lipid densities in the two monolayers. This effect is only relevant at short wavelengths, corresponding to $k > k_C$, the crossover wavenumber given by Eq. 17. Because larger hybrid modes are supported by larger vesicles, the crossover wavenumber is predicted to decrease with the vesicle radius (see Eq. 17). In Figure 8, we plot the values of the crossover wavenumber k_C estimated from the different experiments and analysis methods as a function of the vesicle radius.

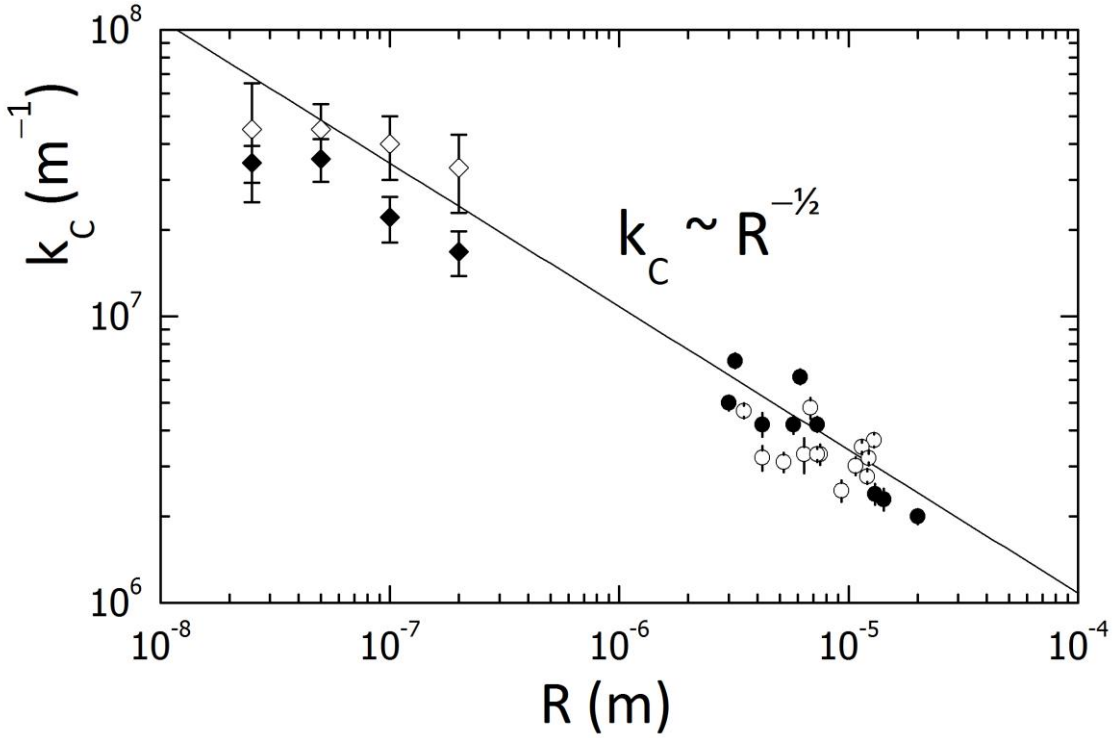

Figure 8. Radius dependence of the crossover wavenumber as determined from vesicles with different sizes. High-*k*) NSE with nanometer sized LUVs (R = 25-200nm). (◇) crossover wave numbers in Fig. 7 (and Fig. SM4a), calculated from fittings of the NSE data to Eq. 32 (and Eq. SM5); (◆) crossover data in Fig. SM4b, alternatively calculated from fits to Eq. SM6 (see Supplementary Material for details). Low-*k*) Flickering spectroscopy with μm-sized GUVs (R = 3-18μm) (○, ●; the different symbols corresponding to vesicles obtained from two different batches). All the data fall into the universal scaling $k_C \sim R^{-1/2}$ predicted from the radius-dependent bimodal spectrum proposed in this work (the straight line corresponds to the theoretical prediction from Eq. 17 taking h = 2nm, K = 0.085N/m and $\kappa = 20k_BT$).

Amazingly, the different data, coming from different experiments and vesicle preparations, depict the $k_C \sim 1/\sqrt{R}$ behavior predicted from our bimodal spectrum. Indeed, the absolute values of the crossover wavenumbers are quantitatively described by Eq. 17 taking the calculated values of the constitutive parameters (see caption in Fig. 8 for details). Particularly interesting is our estimation of the effective thickness, h = 2nm, which represents the distance between centers of force within each monolayer [16]. Clearly, h is less than the structural thickness of the bilayer, a conclusion inherent

to the Helfrich conjecture (see Eq. 9), and broadly accepted in the literature (see Ref. [67] for a recent comprehensive discussion).

V. OUTLOOK AND DIRECTIONS FOR FUTURE WORK

The mechanics of biological membranes is relevant not only to structural aspects in cell biology but also essential to get insight on the physical mechanism of a number of cellular processes involving membrane remodelling. Indeed, biological biomembranes exhibit a rather complex morphology that is primarily determined by the elastic properties of the lipid bilayer and eventually shaped under the action of external forces, e.g. those stressed by the cytoskeleton or by the extracellular matrix. The lipid bilayer of intracellular organelles often have a very complicated topology such as those of the endoplasmatic reticulum or the Golgi apparatus. Likewise, the plasma membrane can develop small buds as those involved in exo- or endocytosis, but also large protrusions and pseudopods that support complex intercellular interactions and processes, such as cell locomotion. A wealth of biophysical information has sustained the idea that the bilayer architecture (with its intrinsic asymmetry) and its dynamics constitute key functional elements of complexity playing a central role on determining cell shapes, maintaining the mechanical resilience of the membrane and providing support to the dynamic processes undergone by the membrane. The concept of spontaneous curvature reflects a possible asymmetry of the membrane, justified either by a different chemical environment on both sides of the membrane or by a different composition of the two monolayers. The spontaneous curvature is usually assumed to determine the local shape of the membrane. However, the idea that dilational and bending stresses are mutually coupled in lipid bilayers could help to understand the global adaptability of the membrane under the dynamic action of the shaping forces. The new physics contained

in this work not only verifies the existence of such curvature-dilational coupling in model bilayers but also open new directions of experimental work in fundamental biophysics and applied physical biology. In the fundamental side, new experiments with vesicles of variable radius can be designed for the simultaneous measurement of the bending and compression moduli in model lipid membranes. The dynamical theory could be used to determine the exact values of the intermonolayer friction coefficient, a material parameter poorly explored in model and real systems. The linear relationship between the compression and bending moduli could be validated with the data arising from the same experiment, and the coupling constant α correlated with the intermonolayer friction as well. This still lacking information is crucial to gain a clever understanding of the role of intrabilayer transport, namely flip-flop motions in real membranes, on the effective coupling between the bilayers. The effective softening produced by the hybrid modes could be efficiently exploited to store mechanical energy in large vesicles. At large wavelengths, the large vesicles should effectively fluctuate tensionless, a feature that can be used to accumulate elastic energy in the larger modes. Regarding dynamical aspects, the presence of the "extraordinary" hybrid mode rivalling with the ordinary bending mode for frictional dissipation opens interesting problems of fundamental physics to be explored with model systems. For instance, the study of the crossover region and the overlapping and possible resonances between the two modes is particularly interesting from the standpoint of statistical physics as models of friction-coupled resonators. The presence of two alternative frictional pathways for energy dissipation offers enormous possibilities for studies of dynamical stability and chaos in multi-stable fluctuating systems with frictional degeneracy. From the experimental standpoint, the modulation of the bulk viscosity appears as an evident parameterization to modulate the time scale of the ordinary bending mode, which is usually faster at large

wavelengths than the hybrid mode. Increasing the solvent viscosity in experiments with giant vesicles seems an obvious experiment to test for the dynamical consequences of mode overlapping in a straightforward realization.

From a more biologically integrative standpoint, the new simplified theory and the proposed methodology could be extremely useful to study complex phenomena such as lipid-protein or lipid-lipid interactions and local phase transitions in model systems, which may deeply influence membrane mechanics. Comprehensive studies of membrane mechanics with cells of defined side are now possible with the new theory including the two relevant modes. The possible functional differences between the two modes could be revealed with a biological significance. The model could be particularly useful in the future to interpret membrane-related phenomena such as protein-promoted membrane perturbations involved in exo-/endocytosis, or the membrane lipid reorganizations underlying the complex topologies of certain organelles, which could ultimately produce measurable deviations from the expected behavior.

VI. CONCLUSIONS

An approximate perturbation theory of the curvature fluctuations has been proposed for spherical vesicles. Assuming the existence of hybrid modes of curvature motion coupling bending with local longitudinal dilations, the theoretical fluctuation spectrum is found with a bimodal form, where the amplitude of the hybrid contribution is predicted to increase linearly with the vesicle radius. This behavior is limited by the natural decoupling of the longitudinal stresses from the normal deflections expected for the planar membrane, which is able to release stress by lipid flow through its free edges. Additionally, we have extended the Zilman-Granek formalism of the structure factor of the bending fluctuations to a bimodal schema compatible with the presence of hybrid

modes competing with pure bending. The precise expression of the dynamic structure factor for the hybrid modes has been obtained from analytical calculations. From the NSE/FS experimental data reported here, the presence of hybrid curvature-longitudinal modes concomitant with the usual tension/bending fluctuations has been clearly evidenced in bilayer vesicles made of DMPC, a phospholipid with two saturated hydrophobic tails of equal length. Such a structural characteristic endows each DMPC monolayer leaflet to slide freely with respect to each other, enabling hybrid modes to relax fast in a similar time scale as the pure bending ones. Such a dynamic congruence allows hybrid modes to effectively couple with pure bending modes resulting in a mechanical interplay leading to an effective softening at the high curvatures involved at high wavevectors. The dynamical features have been probed experimentally over a broad range of vesicle sizes and wavevectors and found in quantitative agreement with the proposed bimodal theory of the curvature fluctuations in bilayer vesicles.

Acknowledgements

This work was funded by MICINN under grants FIS2012-35723, FIS2009-14650-C02-01, Consolider-Ingenio 2010 en "Nanociencia Molecular" (CSD2007-0010), S2013/MIT-2807 (NanoBIOSOMA) and TS2009MAT-1507T (NOBIMAT) from CAM. M. Mell was supported by FPU Program (MEC) and L.H. Moleiro by CSD2007-0010. I. López-Montero thanks support from NOBIMAT (CAM). We gratefully acknowledge ILL Soft Matter Partnership Lab (PSCM@ILL) for DLS-time in its facility and specially to Ralf Schweins for technical assistance.

Appendix: Zilman-Granek formalism for the dynamic structure factor of the membrane fluctuations.

The ZG theory provides us with the analytic formalism for interpreting the dynamic structure factor corresponding to the membrane fluctuations [35,36,66]. The original ZG theory deals with pure bending fluctuations in rigid membranes, but its formalism can be easily generalized to other modes of curvature motion. Here, we describe the main operational details necessary for the calculation of the dynamic structure factor of the membrane fluctuations from the specific trajectories for membrane motion. Indeed, within the respective dynamical description, this general formalism could be applied to curvature modes of any kind. In the most general formulation, in a molecular system, the intermediate scattering function of the internal motions can be expressed as a function of the scattering wavevector **q** as [64],

$$S_{int}(\vec{q},t)/S(\vec{q},0) = \left\langle \sum_{i,j} e^{i\vec{q}\cdot(\mathbf{R}_i(t)-\mathbf{R}_j(0))} \right\rangle \tag{A1}$$

where R_i denotes the position of a given "tagged molecule" in the center-of-mass coordinate frame. Here, the sum runs over all the possible pairs of molecules (i, j) in the scatterer object.

The ZG formalism starts with the general expression in Eq. (A1). Then, because molecular motions have no consequence in scattering at wavelengths longer than the molecular scale and times longer than molecular diffusion, a continuous description of the membrane motions is adopted in the hydrodynamic regime. In the ZG description, the molecular index i is replaced by the topological position (r) on the membrane surface. ZG considered a single membrane whose neutral plane makes an arbitrary angle with the scattering wavevector **q**. For the shape fluctuations, only the normal displacements with respect to the neutral plane are active in producing scattering, the normal deviation $h(r,t)$ defining the only relevant displacement. For isotropic phases, such as the vesicle phase, the powder-like structure factor is calculated as an average

over all angles between **q** and the normal vector to the base plane of the membrane, thus the dominating region of integration corresponds to membrane orientations perpendicular to the scattering wavevector. Under these conditions, the general expression in Eq. A1 can be then rewritten as [36]:

$$S_{fluct}(q,t)/S(q,0) = \left\langle \sum_{i,j} e^{iq\cdot\left(h_i(t)-h_j(0)\right)} \right\rangle \tag{A2}$$

Once assumed a continuous description, the dynamical correlations are described by the relative displacements between two separated points in the fluctuating membrane. Then, in the continuum limit, the double sum over molecules in Eq. (A2) becomes a double sum over the internal membrane curvilinear coordinate [36]:

$$S_{fluct}(q,t)/S(q,0) = \int\int \left\langle e^{iq\left(h(r,t)-h'(r',0)\right)} \right\rangle dr dr' \tag{A3}$$

In the ZG theory, $S_{fluct}(k,t)$ is assumed to arise from correlations in the relative positions of different points in the membrane, thus the calculation of the dynamic structure factor implies an average over the different pairs in the membrane. Because thermal fluctuations obey Gaussian statistics, by a general theorem of stochastic processes [68], such an ensemble average can be calculated as a Gaussian distribution of the averaged fluctuations, this is $\langle exp(iq\Delta h(t))\rangle = exp(-q^2\langle \Delta h^2(t)\rangle/2)$ where the two-point correlation function has been defined as $\langle \Delta h^2\rangle = \langle (h(r,t)-h'(r',0))^2\rangle$. Consequently, one should rather focus in the two-point correlation function, which is the relevant quantity for the subsequent calculation of the intermediate scattering function corresponding to the shape fluctuations [36], this is:

$$S_{fluct}(q,t)/S(q,0) = \int\int \exp\left[-\frac{q^2}{2} \left\langle \left(h(r,t) - h'(r',0) \right)^2 \right\rangle \right] dr dr' \tag{A4}$$

We are specifically interested in two-point correlations, thus precise relationships with the correlation functions in each single-point are required. Particularly, for the relevant two-point correlation function, in real space, one finds:

$$\left\langle \left(h(r,t) - h'(r',0) \right)^2 \right\rangle = \left\langle h^2(r,t) \right\rangle + \left\langle h'^2(r',0) \right\rangle - 2\left\langle h(r,t) h'(r',0) \right\rangle \qquad \text{(A5)}$$

In the following and for the best convenience to work in reciprocal space, the stochastic field $h(r,t)$ will be expressed in terms of Fourier modes:

$$h(r,t) = \frac{1}{2\pi} \int h_q(t) e^{ikr} dk \qquad \text{(A6)}$$

where k is the 2D fluctuation wavevector of the membrane undulation modes. So, for the relevant two-point correlation function in Eq. A5, in Fourier space, one can rewrite:

$$\begin{aligned} &\left\langle \left(h(r,t) - h'(r',0) \right)^2 \right\rangle = \\ &= \frac{1}{4\pi^2} \iint \left[\left\langle h_{\mathbf{k}}(t) h_{-\mathbf{k}}(t) \right\rangle + \left\langle h_{\mathbf{k}}(0) h_{-\mathbf{k}}(0) \right\rangle - 2\left\langle h_{\mathbf{k}}(t) h_{-\mathbf{k}}(0) \right\rangle e^{iq(r-r')} \right] d^2k \end{aligned} \qquad \text{(A7)}$$

Since thermal fluctuations are a stationary stochastic process, ergodicity imposes $\langle h_k^2(t) \rangle = \langle h_k^2(0) \rangle = \langle h_k^2 \rangle$. Likewise, thermal modes are characterised by exponential correlations $\langle h_k(t) h_k(0) \rangle = \langle h_k^2 \rangle \, e^{-\gamma(k)t}$, with a relaxation rate defined by a k-dependent dispersion, $\gamma(k)$ which is defined as a dynamical ratio of the corresponding restoring force to the viscous dissipation. Moreover, the ZG theory assumes cyclic boundary conditions, which make the spatial dependence of $\langle (h(r,t) - h'(r',0))^2 \rangle$ dependent only on the difference $r - r'$, but not on the absolute positions. Therefore, Eq. A7 can be re-written in the general form [36]:

$$\left\langle \left(h(r,t) - h'(r',0) \right)^2 \right\rangle = \left\langle \Delta h^2(r - r', t) \right\rangle = \frac{1}{2\pi^2} \iint \left\langle h_k^2 \right\rangle \left(1 - e^{ik(r-r')} e^{-\gamma(k)t} \right) d^2k \qquad \text{(A8)}$$

On the one hand, the time-independent part of the two-point relative displacements can be obtained as a static correlator ($t = 0$) defined as:

$$\phi_0\left(r-r'\right)=\left\langle \Delta h^2\left(r-r',t=0\right)\right\rangle=\frac{1}{2\pi^2}\int\int\left\langle h_k^2\right\rangle\left(1-e^{ik(r-r')}\right)d^2k \tag{A9}$$

On the other hand, a dynamic correlator, which contains the relevant time dependence, can be defined as:

$$\phi\left(r-r',t\right)=\frac{1}{2\pi^2}\int\int\left\langle h_k^2\right\rangle e^{ik(r-r')}\left(1-e^{-\gamma(k)t}\right)d^2k \tag{A10}$$

in a way such that Eq. (A8) can be re-written as the sum of the two terms [36]:

$$\left\langle \Delta h^2\left(r-r',t\right)\right\rangle=\phi_0\left(r-r',0\right)+\phi\left(r-r',t\right) \tag{A11}$$

For small distances, $r–r'\rightarrow 0$, static correlations are found with an asymptotic quadratic dependence, $\phi_0 \sim (r - r')^2$ [36], a well known result indicating that the height difference between two points on the membrane is essentially proportional to the lateral distance between them [4]. However, the more relevant result concerns to $\phi(r - r', t)$ which will determine the time dependence of the fluctuation structure factor.

For pure bending modes one has $\langle h_k^2\rangle_{bend} = k_BT/\kappa k^4$ and $\gamma_{bend} = (\kappa/4\eta)k^3$; so, after a variable change, $z = \xi k$, which is written in terms of a characteristic, time-dependent, bending length, $\xi = (\kappa t/4\eta)^{1/3}$, the integral in Eq. A10 can be re-written as follows [36]:

$$\phi\left(r-r',t\right)=\frac{1}{2\pi^2}\left[\frac{1}{4}\left(\frac{k_BT}{\kappa}\right)^{1/2}\frac{k_BT}{\eta}t\right]^{2/3}F\left[\left(r-r'\right)/\xi\left(t\right)\right] \tag{A12}$$

where $F[u(t)]$ was defined as:

$$F\left[u\left(t\right)\right]=\int_0^\infty\int_0^\infty e^{iu(t)z}\frac{1-e^{-z^3}}{z^4}d^2z \tag{A13}$$

with $u(t)$ being a monotonically decaying function of the dimensionless lateral distance:

$$u\left(t\right)=\frac{r-r'}{\xi\left(t\right)}=\frac{r-r'}{\left(\kappa t/4\eta\right)^{1/3}} \tag{A14}$$

This function can be calculated numerically, although the relevant asymptotic limit can be analytically discussed. Over short distances ($u < 1$), $F(u)$ decays near-quadratic with increasing u, the asymptotic form being [36]:

$$F(u) \approx 1.34 + (0.25 \ln u - 0.33) u^2 + o(u^4) \tag{A15}$$

Consequently, in the $u \to 0$ limit, the scaling function is constant $F(u) \approx 1.34 \sim t^0$, so point-to-point correlations are expected with a main time dependence arisen from the variable change implicit to Eq. A12. Therefore, for the two-point correlations in rigid vesicles governed by bending modes, one expects a sub-diffusive trajectory varying with time as [35,36,66]:

$$\left\langle \Delta h^2(t) \right\rangle_{bend} \approx \phi(u \to 0, t) \approx 0.025 \left[\left(\frac{k_B T}{\kappa} \right)^{1/2} \frac{k_B T}{\eta} t \right]^{2/3} \tag{A16}$$

Consequently, if one looks at the time dependence of the dynamic structure factor of the bending fluctuations, substituting Eq. A16 into Eq. A4, one finds a stretched exponential profile as:

$$S_{fluct}(q,t) / S_{fluct}(q,0) \approx \exp\left[-(\Gamma_{bend} t)^{2/3} \right] \tag{A17}$$

with a decay rate:

$$\Gamma_{bend}(q) \approx 0.025 \left(\frac{k_B T}{\kappa} \right)^{1/2} \frac{k_B T}{\eta} q^3 \tag{A18}$$

This constitutes the major result of the ZG theory, which introduces the sub-diffusive character of the bending fluctuations in rigid membranes as a main feature defining the relaxation of the dynamic structure factor. For transversal fluctuation modes of any other nature, *e.g.* hybrid modes coupling transverse bending with longitudinal stresses, the general formalism remains still applicable (Eqs. A1-A11), but the specific expressions for the mode amplitudes and relaxation rates must be explicitly considered

in Eqs. A9-A11. The new expressions for the dynamic structure factor corresponding to hybrid modes have been included in the main text of this paper.

REFERENCES

[1] S. J. Singer and G. L. Nicolson, Science **175**, 720 (1972).

[2] M. P. Sheetz and S. J. Singer, Proc. Natl. Acad. Sci. U.S.A. **71**, 4457 (1974).

[3] E. Sackmann, H.P. Duwe, K. Zeman and A. Zilker, in *Structure and Dynamics of Nucleic Acids, Proteins and Membranes*, edited by E. Clementi and S. Chin (Plenum, New York, 1986), p. 251.

[4] S.A. Safran, Statistical Thermodynamics of Surfaces, Interfaces and Membranes, Addison-Weley, New York (1994).

[5] U. Seifert, K. Berndl and R. Lipowsky, Phys. Rev. A **44**, 11182 (2001).

[6] L. Kramer, J. Chem. Phys. **55**, 2097 (1971).

[7] M. B. Schneider, J. T. Jenkins, and W. W. Webb, J. Phys. (Paris) 45, 1457 (1984).

[8] S.T. Milner, S.A. Safran, Phys. Rev. A **36**, 4371 (1987).

[9] A.J. Levine, F.C. MacKintosh, Phys. Rev. E **66**, 061606 (2002).

[10] B.A. Camley, F.L.H. Brown, Phys. Rev. E **84**, 021904 (2011).

[11] R. Granek, Soft Matter 7, 5281 (2011).

[12] T. Betz, Soft Matter 8, 5317 (2012).

[13] W. Helfrich, Z. Naturforschung **28c**, 693 (1973).

[14] D.A. Boal, *Mechanics of the Cell*, 2nd ed., Cambridge Univ. Press, Cambridge (2012).

[15] W. Helfrich, Z. Naturfosch, **29c**, 510 (1974).

[16] E. Evans, A. Yeung, R. Waugh, J. Song, in *Structure and Conformation of Amphiphilic Membranes*, R. Lipowsky, D. Ritcher and K. Kremer, eds. (Springer, Berlin, 1992) pp. 146-153.

[17] A. Yeung and E. Evans, J. Phys. II **5**, 1501 (1995).

[18] R. Lipowsky, Nature **349**, 475 (1991).

[19] R. Rodríguez-García, L. R. Arriaga, M. Mell, L. H. Moleiro, I. López-Montero, F. Monroy, Phys. Rev. Lett. 102, 128201 (2009).

[20] P. Méléard, M. D. Mitov, J. F. Faucon and P. Bothorel. Europhys. Lett. 11, 355 (1990).

[21] T. Pott and P. Méléard, Europhys. Lett. 59, 87 (2002).

[22] L.R. Arriaga, I. López-Montero, G. Orts-Gil, B. Farago, T. Hellweg, F. Monroy, Phys. Rev. E **80**, 031908 (2009).

[23] L.R. Arriaga, R. Rodríguez-García, I. López-Montero, B. Farago, T. Hellweg, F. Monroy, Eur. Phys. J. E **31**, 105–113 (2010).

[24] R.M. Raphael and R.E. Waugh, Biophys. J. 71, 1374 (1996).

[25] R. Merkel, E. Sackmann and E. Evans, J. Phys. (Paris), 50, 1535 (1989).

[26] U. Seifert and S.A. Langer, Europhys. Lett. **23**, 71 (1993).

[27] M. Kraus and U. Seifert, J. Phys. II France **4**, 1117 (1994).

[28] M.C. Watson and F.L.H. Brown, Biophys. J. 98**,** L9-L11 (2010).

[29] W. Rawicz, K.C. Olbrich, T. McIntosh, D. Needham, and E. Evans, Biophys. J. **79**, 328 (2000).

[30] "Theory of Elasticity", Course of Theoretical Physics, vol.7. L.D. Landau and E.M. Lifshitz (Butterworth -Heinemann, UK, 1986)

[31] M. Mell, L.H. Moleiro, Y. Hertle, P. Fouquet, R. Schweins, I. López-Montero,T. Hellweg and F. Monroy. Eur. Phys. J. E **36**, 75 (2013).

[32] S.A. Shkulipa, W.K. den Otter and W.J. Briels, Phys. Rev. Lett. **96**, 178302 (2006).

[33] M.C. Watson, E.G. Brandt, P.M. Welch and F.L.H. Brown, Phys. Rev. Lett. **109**, 028102 (2012).

[34] J. Pécréaux, H.G. Döbereiner, J. Prost, J.-F. Joanny, P. Bassereau, Eur. Phys. J. E 13, 277 (2004).

[35] A.G. Zilman and R. Granek, Phys. Rev. Lett. **77**, 4788 (1996).

[36] A.G. Zilman and R. Granek, Chem. Phys. **284**, 195 (2002).

[37] T. Takeda et al., J. Phys. Chem. Solids **60**, 1375 (1999)

[38] M. Nagao et al., J. Appl. Crystallogr. **33**, 653 (2000).

[39] S. Komura, T. Takeda, Y. Kawabata, S.K. Ghosh, H. Seto and M. Nagao, Phys. Rev. E **63**, 041402 (2001).

[40] E. Freyssingeas, D. Roux, F. Nallet, J. Physique 7 (1997) 913.

[41] Y. Kimura, J. Oizumi, R. Hayakawa, Mol. Cryst. Liq. Crys. A 332 (1999) 3069.

[42] A.C. Woodka, P.D. Butler, L. Porcar, B. Farago, M. Nagao, Phys. Rev. Lett. **109**, 058102 (2012).

[43] B. Brüning, R. Stehle, P. Falus and B. Farago. Eur. Phys. J. E, 36, 77 (2013).

[44] W. Helfrich and R.M. Servuss. Nuovo Cimento D **3**, 137 (1984).

[45] M. D. Schneider, J. T. Jenkins, and W. W. Webb, J. Phys. (Paris) **45**, 1457 (1984)

[46] "Thin Plates and Shells", E. Ventsel, Th. Krauthammer (Marcel-Dekker, NY, 2001).

[47] D. Marsh, Chem. Phys. Lipids **144**, 146 (2006).

[48] J. F. Faucon, M. D. Mitov, P. Meleard, I. Bivas, and P. Bothorel, J. Phys. (Paris) **50**, 2389 (1989).

[49] L. Miao, M.A. Lomholt and J. Kleis, Eur. Phys. J E **9**, 143 (2002).

[50] I. Bivas, Phys. Rev. E **81**, 061911 (2010).

[51] M. Angelova, S. Soleau, P. Meleard, F. Faucon, P. Bothorel. Prog. Colloid. Polym. Sci., 89, 127 (1992)

[52] L. Mathivet, S. Cribier, P. Devaux. Biophys. J. **70**, 1112 (1996)

[53] B.J. Frisken, C. Asman, P. J. Patty. Langmuir **16**, 928 (2000)

[54] S. W. Provencher, Computer Physics Com. **27**, 213 (1982); *ibid.* **27**, 229 (1982).

[55] A. Jakes, Collect. Czech. Chem. Commun. **60**, 1781 (1995).

[56] B. Farago. Physica B: Cond. Matter **385-386**, 688 (2006).

[57] P. Schleger, et al., Physica B **266**, 49 (1999).

[58] L.R. Arriaga, I. López-Montero, F. Monroy, G. Orts-Gil, B. Farago, T. Hellweg, Biophys. J. 96, 3629 (2009).

[59] *Bending Rigidities of Lipid Bilayers: Their Determination and Main Inputs in Biophysical Studies* by H. Bouvrais, Chapter 1 in *Advances in Planar Bilayers and Liposomes*, Vol. 15, Elsevier (2012).

[60] L.R. Arriaga, R. Rodríguez-García, I. López-Montero, B. Farago, T. Hellweg, F. Monroy, Eur. Phys. J. E **31**, 105 (2010).

[61] In a flat surface, $C \approx \nabla^2\zeta \approx k^2\zeta$, so $\delta C \approx k^2\delta\zeta$; considering the Helfrich's conjecture, $\delta C \approx 2\delta u/h$, one gets $\delta\zeta/\delta u \approx 2/hk^2$, as predicted by Eq. 14 in the limit $R \rightarrow \infty$.

[62] R.M. Raphael and R.E. Waugh, Biophys. J. **71**, 1374 (1996).

[63] R. Merkel, E. Sackmann and E. Evans, J. Phys. (Paris) **50**, 1535 (1989).

[64] B. J. Berne and R. Pecora, *Dynamic Light Scattering* (Wiley, New York, 1976).

[65] S. W. Lovesey and P. Schofield, J. Phys. C: Solid State Phys. **9**, 2843 (1976).

[66] R. Granek, J. Phys. II (France) **7**, 1761 (1997).

[67] N.G. van Kampen, Stochastic Process in Physics and Chemistry, North-Holland, Amsterdam (1992).

[68] J.F. Nagle, Faraday Discuss. 161, 11 (2013).